
Absorption Spectroscopy and Electron Diffraction for the Characterisation of an Ultramicrotome Prepared nm-Thin Organic Molecular Rubrene Crystal

by

Michiel Jozef Leonardus Jansen

Fontys University of Applied Sciences,
Engineering Physics

&

Max Planck Institute
for the Structure and Dynamics of Matter

June 2022

A thesis submitted for the degree of
Bachelor of Science



Absorption Spectroscopy and Electron Diffraction for the Characterisation of an Ultramicrotome Prepared nm-Thin Organic Molecular Rubrene Crystal

Author

Michiel Jozef Leonardus Jansen
michiel.jansen2803@gmail.com
michiel.jansen@student.fontys.nl
+31 6 40530437

Education

Fontys University of Applied Sciences
Engineering Physics
Rondom 1
5612 AP, Eindhoven
The Netherlands

Academic Supervisor

Dr. Albert Bart Smit
ab.smit@fontys.nl
+31 08850 83224

Duration

February 1, 2022 – June 30, 2022

Date of Submission

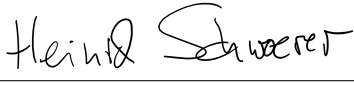
June 13, 2022

Institute

Max Planck Institute
for the Structure and Dynamics of Matter
Luruper Chaussee 149
22761, Hamburg
Germany

Institute Supervisor

Dr. Heinrich Schwoerer
heinrich.schwoerer@mpsd.mpg.de
+49 040 8998 88281

Approved: 
Hamburg, June 10, 2022

Prologue

The bachelor thesis in front of you is written as part of the education Engineering Physics of Fontys University of Applied Sciences in Eindhoven and the graduation internship for the degree of Bachelor of Science. The internship was executed at the Max Planck Institute for the Structure and Dynamics of Matter in Hamburg, Germany in the period of February 1 until June 30, 2022.

I have been lucky enough to have come in contact with scientists within the Max Planck Institute in Hamburg. These skilful scientists have, from day one, made it their mission to teach me as much about the scientific world and scientific research as possible. For that, I am most grateful.

This research would not have been successful without the help and teachings of Dr. Heinrich Schwoerer and Dr. Gabriele Tauscher. They were most patient explaining everything that was necessary. Moreover, they were enthusiastic to guide a student in his time in Hamburg. A student could not wish for better guidance or warmer people. Further, I want to acknowledge Dr. Bart Smit whom mentioned this great opportunity and whom was ever interested in the project's progress. Lastly, I want to mention all other employees of the Max Planck Institute who made my time in Hamburg most memorable.

Thank you, Dank jullie wel, Danke schön.

Sincerely,

Michiel Jansen

A handwritten signature in black ink, consisting of a series of loops and strokes, representing the name Michiel Jansen.

Hamburg, June 10, 2022

Summary

Within the Max Planck Institute for the Structure and Dynamics of Matter, an experiment is commencing to study the behaviour of organic crystals at various temperatures ranging from room temperature down to approximately 10 K. This experiment encompasses Transient Absorption Spectroscopy (TAS) and Ultrafast Electron Diffraction (UED). TAS en UED measurements use a pump-probe set-up to observe the behaviour of an organic crystal as a function of time. The goal of TAS experiments is to explore electronic transitions in the context of organic electronics and excitonic studies, important to charge transport in organic-crystal-based semiconductors. The structure of the crystal (i.e. its crystallographic order) can be deduced from UED experiments. In the TAS and UED experiments, rubrene is pumped from the electronic ground state into an excited state by an ultrashort laser pulse in the order of a few tens of femtoseconds. While the overall research will study the excited states of an organic molecular rubrene crystal, shall this thesis focus on characterising the ground state of rubrene using absorption spectroscopy and electron diffraction.

Rubrene is an organic molecule containing a single tetracene compound with four separate benzene compounds attached to the sides and rotated 90° on the horizontal plane. From the molecular orbital theory, we learn that the π -orbitals of tetracene all ‘fuse’ together to a single π -orbital. The same applies for the benzene compounds. The fused π -orbitals is what gives rubrene its semiconductor properties.

Incident light on a solid crystal must either scatter, reflect or transmit. Light traversing the crystal can be absorbed by the rubrene molecules, thereby exciting molecules into higher electronic states. The optical properties of the crystal are important for absorption spectroscopy as transmittance and absorbance are both also wavelength dependant per crystal. In the case of an electron traversing the crystal, scattering at the molecules of the crystal lattice can occur. Dependent on the electrons’ speed and the thickness of the crystal layer seen by the electron, the electron can be scattered, transmitted, or diffracted. The latter is the interference of the electron waves after exiting the crystal. The only dependence of electron scattering is the crystallography of rubrene and the electron speed.

The interaction of rubrene with photons and electrons, as is used in absorption spectroscopy and electron diffraction, respectively, can only be observed for very thin sample slices of the rubrene crystal, as the crystal thickness is restrictive to the transmittance of both light and electrons. The rubrene crystals are cut using an ultramicrotome which is capable of slicing sample suitable for the above mentioned experiments which is in the order of 100 nm.

In this work, absorption spectroscopy has been conducted in two states of matter: dissolved and crystallised rubrene. Rubrene was dissolved in chloroform. Three concentration of the solution were made $c = 0.1, 0.05, 0.01$ mmol/L. These three solutions showed the same peak absorption wavelengths in the visible spectrum at $\lambda = 529.5, 494, 465, 436$ nm and a vibronic progression of $\Delta k = 1350$ cm⁻¹. Crystallised rubrene was cut in three thicknesses $t = 250, 200, 150$ nm. All the spectra of crystallised rubrene showed the same peak absorption wavelengths in the visible spectrum at $\lambda = 536, 501, 467, 441, 415.5$ nm. The peak absorption wavelengths were found to be redshifted with respect to the peak absorption wavelengths of dissolved rubrene with an average of $\Delta\lambda_r = 5$ nm redshift. Also, a similar vibronic progression of $\Delta k = 1353$ cm⁻¹ was observed.

The electron diffraction experiment is conducted in a diffractometer. In this diffractometer, an electron beam is produced, accelerated by an electric field and focused by a magnetic field. After the electrons are transmitted through and scattered by the thin sample, the electrons will strike a phosphorescent screen. The phosphor particles convert the kinetic energie of the electrons into visible light, which is captured by a CCD (Charge-Coupled Device). Two crystals were examined in the diffractometer. They were then visually and objectively compared with simulations by commercial software CrystalMaker and SingleCrystal. Crystal A3 visually showed resemblance to crystal orientation A. The ratios of consecutive diffraction maxima horizontally (H) and vertically

(V) have been determined to be $H/V = 2.00$ and $V/H = 0.500$, which also corresponded well with the ratios of orientation A's simulations. The Crystal B1 visually showed resemblance to crystal orientation C. The ratio between consecutive diffraction maxima horizontally and vertically have been determined to be $H/V = 0.272$ and $V/H = 3.68$, which also corresponded well with the ratios of orientation C's simulations.

Samenvatting

In het Max Planck Instituut voor de Structuur en Dynamica van Materie wordt een onderzoek opgestart om het gedrag van organische kristallen op verscheidene temperaturen van kamertemperatuur tot ongeveer 10 K te bestuderen. Hieronder valt Transient Absorption Spectroscopy (TAS) en Ultrafast Electron Diffraction (UED). TAS en UED metingen gebruiken een pump-probe opstelling om het gedrag van een organisch kristal als functie van tijd te observeren. Het doel van TAS experimenten is om de elektronische transitie in kader van organische elektronica en excitonische studies welke belangrijk zijn voor ladingtransport in organisch- en kristal-gebaseerde halfgeleiders. De structuur van het kristal (de kristallografische orde) kan worden afgeleid van UED experimenten. In de TAS en UED experimenten wordt rubrene gepompt vanaf de elektronische grondtoestand naar hogere excitatietoestanden door een ultrakorte laserpuls in de orde van tientallen femtoseconden. Terwijl het overkoepelende onderzoek de excitatietoestanden van een organisch moleculair rubreenkristal onderzoekt, zal deze scriptie zich focussen op de karakterisatie van de grondtoestand van rubreen met behulp van absorptiespectroscopie en elektrondiffractie.

Rubreen is een organisch molecuul dat één enkel tetraceenverbinding bevat met vier aparte benzeenverbindingen welke ieder 90° ten opzichte van het horizontale vlak zijn geroteerd. Van de molecuulorbitalentheorie leert men dat de π -orbitalen van tetraceen worden 'gefuseerd' naar één π -orbitaal. Hetzelfde geldt voor de benzeenverbindingen. De gefuseerde π -orbitalen is hetgeen dat rubreen halfgeleideigenschappen geeft.

Inkomend licht op een solide kristal moet worden verstrooid, gereflecteerd of worden doorgelaten. Licht dat door het kristal gaat kan door de rubreenmoleculen worden geabsorbeerd, waardoor moleculen naar hogere elektronische toestanden worden geëxciteerd. De optische eigenschappen van het kristal zijn belangrijk voor absorptiespectroscopie, omdat transmissie en absorptie beide golflengteafhankelijk zijn per kristal. In het geval van elektronen die door het kristal gaan, kan verstrooiing bij de moleculen van het kristalrooster optreden. Afhankelijk van de elektronensnelheid en de dikte van de kristallaag gezien door het elektron kan het elektron worden verstrooid, doorgelaten of gebogen. De laatste is de interferentie van de elektrongolven na verlaat van het kristal. De enige afhankelijkheid van elektronverstrooiing is de kristallografie van rubreen en de elektronensnelheid.

De interactie van rubreen met fotonen en elektronen, zoals in absorptiespectroscopie en elektrondiffractie, respectievelijk, kan slechts worden geobserveerd bij zeer dunne monstersneden van het rubreenkristal, omdat de kristaldikte restrictief is voor de transmissie van zowel licht als elektronen. De rubreenkristallen zijn gesneden met behulp van een ultramicrotome, een apparaat dat in staat is kristalmonsters te snijden welke geschikt zijn voor de experimenten in de orde van 100 nm ligt.

In dit werk is absorptiespectroscopie uitgevoerd in twee materietoestanden: opgelost en gekristalliseerd rubreen. Rubreen is opgelost in het oplosmiddel chloroform. Hiervan zijn drie concentraties gemaakt $c = 0.1, 0.05, 0.01$ mmol/L. Deze drie oplossingen lieten dezelfde piek absorptiegolflengten zien in het zichtbare spectrum op $\lambda = 529.5, 494, 465, 436$ nm en een vibronische progressie van $\Delta k = 1350$ cm^{-1} . Gekristalliseerd rubreen is gesneden in drie diktes $t = 250, 200, 150$ nm. Al deze spectra van gekristalliseerd rubreen lieten dezelfde piek absorptiegolflengten zien in het zichtbare spectrum op $\lambda = 536, 501, 467, 441, 415.5$ nm. De absorptiepieken bleken een roodverschuiving ten opzichte van de absorptiepieken van de rubreenoplossingen te bevatten van gemiddeld $\Delta\lambda_r = 5$ nm. Daarnaast is ook een vergelijkbare vibronische progressie van $\Delta k = 1353$ cm^{-1} geobserveerd.

Het elektronendiffractie experiment is uitgevoerd in een diffractometer. In deze diffractometer wordt een elektronenstraal geproduceerd, versneld door een elektrisch veld en gefocust door een magnetisch veld. Nadat de elektronen worden doorgelaten en verstrooid door het dunne rubreenmonster, zullen de elektronen botsen op een fosforescerend scherm. De forfordeeltjes converteren de kinetische energie van de elektronen naar zichtbaar licht wat wordt opgevangen door een CCD (Charge-Coupled Device). Twee kristallen zijn onderzocht in de diffractometer. Deze zijn visueel en objectief vergeleken met simulaties door commercieel software CrystalMaker en SingleCrystal. Kristal A3 toonde een gelijkenis met kristaloriëntatie A. De ratio's van opeenvolgende diffractiemaxima horizontaal (H) en verticaal (V) zijn bepaald op $H/V = 2.00$ en $V/H = 0.500$ welke goed overeenkwamen met de ratio's van de simulaties van oriëntatie A. Kristal B1 toonde een gelijkenis met kristal oriëntatie C. De ratio's van opeenvolgende diffractiemaxima horizontaal en verticaal zijn bepaald op $H/V = 0.272$ en $V/H = 3.68$ welke goed overeenkwamen met de ratio's van de simulaties van oriëntatie C.

Zusammenfassung

Im Max-Planck-Institut für Struktur und Dynamik der Materie wird Forschung zum Verhaltens von organischen Kristallen bei diversen Temperaturen von Raumtemperatur bis zu ungefähr 10 K betrieben. Experimente umfassen Transient Absorption Spectroscopy (TAS) und Ultrafast Electron Diffraction (UED). TAS- und UED-Messungen benutzen die sogenannte Pump-probe Methode um das Verhalten eines organischen Kristalls als Funktion der Zeit zu untersuchen. Das Ziel der TAS-Experimente ist die Erforschung elektronischer Übergänge im Kontext der organischen Elektronik und exzitonische Studien, die für den Ladungstransport in Halbleitern auf organischer und kristallbasis wichtig sind. Der Struktur des Kristalls (kristallographische Ordnung) kann von UED-Experimenten abgeleitet werden. In den TAS- und UED-Experimenten wird Rubren mit einem ultrakurzen Laserpuls in der Größenordnung von einigen zehn Femtosekunden vom elektronischen Grundzustand in einen angeregten Zustand gepumpt. Während die gesamte Forschung angeregte Zustände des Rubren Kristalls untersucht, soll diese Thesis sich fokussieren auf die Charakterisierung mit Absorptionsspektroskopie und Elektronenbeugung des Grundzustands von Rubren.

Rubren ist ein Molekül mit einer Tetracenverbindung und vier getrennte Benzolverbindungen, welche an der Seiten des Tetracens verbunden. Von der Molekülorbitaltheorie lernt man, dass die π -Orbitale des Tetracens zu einem einzigen Orbital 'fusionieren'. Das Gleiche gilt für die Benzolverbindungen: die fusionierten π -Orbitale sind das was Rubren Halbleitereigenschaften gibt.

Auf einen soliden Kristall Einfallendes Licht muss entweder streuen, reflektieren oder transmittieren. Licht, das durch den Kristall geht kann von den Rubrenmolekülen absorbiert werden und damit Moleküle zu höheren elektronischen Zuständen anregen. Die optischen Eigenschaften des Kristalls sind wichtig für Absorptionsspektroskopie, weil Durchlässigkeit und Absorbanz beide wellenlängenabhängig für einen spezifischen Kristall sind. Beim durchqueren eines Kristalls kann ein Elektron an der Kristallgitters gestreut werden. Abhängig von der Geschwindigkeit der Elektronen und der Dicke der Kristallschicht, die das Elektron sieht, kann das Elektron gestreut, durchgelassen oder gebeugt werden. Letzteres ist die Interferenz der Elektronenwellen nach dem Verlassen des Kristalls. Die Elektronenstreuung hängt dabei von der Kristallographie des Rubrens und der Elektronengeschwindigkeit ab.

Die Interaktion des Rubrens mit Photonen und Elektronen, die in Absorptionsspektroskopie und Elektronenbeugung beobachtet werden kann, erfordert sehr dünne Probeschnitte des Rubrenkristalls, weil die Kristalldicke restriktiv ist für den Durchlässigkeit von Licht und Elektronen. Der Rubrenkristall wird mit einem Ultramicrotome geschnitten, ein Gerät, das Proben auf die gewünschte Dicke für die Experimente schneiden kann, die in der Größenordnung von 100 nm liegt.

In dieser Arbeit ist Absorptionsspektroskopie in zwei Materiezustände durchgeführt: in einer Lösung und kristallisiertes Rubren. Rubrene ist in dem Lösungsmittel Chloroform aufgelöst und drei

Konzentrationen sind gemacht worden: $c = 0.1, 0.05, 0.01$ mmol/L. Diese drei Lösungen zeigten in dem sichtbaren Spektrum dieselbe Absorptionsspitzen auf: $\lambda = 529.5, 494, 465, 436$ nm und eine vibronische Progression von $\Delta k = 1350$ cm⁻¹. Kristallisiertes Rubren ist in drei Dicken geschnitten: $t = 250, 150, 150$ nm. Alle Spektren des Rubrens zeigten dieselbe Absorptionsspitze auf: $\lambda = 536, 501, 467, 441, 415.5$ nm. Alle Absorptionsspitze scheinen eine Rotverschiebung hinsichtlich der Absorptionsspitze der Rubrenlösungen von durchschnittlich $\Delta\lambda_r = 5$ nm zu enthalten. Auch ist eine vibronische Progression von $\Delta k = 1353$ cm⁻¹ beobachtet worden.

Das Elektronenbeugungsexperiment ist mit einem Diffraktometer gemacht. In diesem Diffraktometer wird ein Elektronenstrahl produziert, mit einem elektrischen Feld beschleunigt und mit einem magnetischen Feld fokussiert. Nachdem die Elektronen transmittiert und gestreut sind durch die dünne Rubrenprobe, sollen die Elektronen auf einen phosphoreszierenden Schirm fallen. Die Phosphorteilchen konvertieren die kinetische Energie der Elektronen zu sichtbarem Licht, welches von der CCD (Charge-Coupled Device) erfasst wird. Zwei Kristalle sind im Diffraktometer untersucht. Diese wurden visuell und objektiv mit Simulationen von der kommerziellen Software CrystalMaker und SingleCrystal verglichen. Kristall A3 zeigte visuelle Ähnlichkeit mit Kristallorientierung A. Die Verhältnisse der konsekutiven horizontalen (H) und vertikalen (V) Maxima ist auf $H/V = 2.00$ und $V/H = 0.500$ festgestellt, was den Simulationen der Orientierung A entspricht. Kristall B1 zeigte visuell Ähnlichkeit mit Kristallorientierung C. Die Verhältnisse der konsekutiven horizontalen und vertikalen Maxima ist auf $H/V = 0.272$ und $V/H = 3.68$ festgestellt, was den Simulationen der Orientierung C entspricht.

Terminology

This terminology contains used abbreviations, and symbols from the Latin and Greek alphabet from throughout the thesis. All are in alphabetic and chronological order.

Abbreviations

C	Carbon	MPSD	Max Planck Institute for the Structure and Dynamics of Matter
CCD	Charge-Coupled Device	LUMO	Lowest Unoccupied Molecular Orbital
C ₄₂ H ₂₈	Rubrene	N	Nitrogen
CHCl ₃	Chloroform	O	Oxygen
IR	Infrared	OLED	Organic Light Emitting Diodes
H	Hydrogen	TAS	Transient Absorption Spectroscopy
He	Helium	TEM	Transmission Electron Microscope
HOMO	Highest Occupied Molecular Orbital	UED	Ultrafast Electron Diffraction
H/V	Horizontal-vertical ratio	UV	Ultra Violet (spectrum)
Li	Lithium	V/H	Vertical-horizontal ratio
M	Mirror	Vis	Visible (spectrum)

Latin

a	Edge length unit cell [\AA]	m	Mass [kg]
A	Absorbance [OD] (i.e. optical density)	m_l	Magnetic quantum number
b	Edge length unit cell [\AA]	m_s	Magnetic spin quantum number
b	Slit width [m]	n	Principle quantum number
c	Edge length unit cell [\AA]	N	Total amount $N \in \mathbb{N}$
c	Concentration [mmol/L] or [mol/m ³]	p	p-orbital
d	Distance [m]	p	Momentum [kg·m/s]
e^-	Electrons	s	s-orbital
E	Energy [J]	s	Separation distance between slits [m]
E	Electric field [N/m]	t	Sample thickness [nm]
h	Planck's constant [J·s]	T	Transmittance [-]
\hbar	Dirac's constant [J·s]	U	Acceleration voltage [kV]
I_0	Incoming light intensity [W/m ²]	v	Velocity [m/s]
I	Measured light intensity [W/m ²]	V	Potential energy [J]
k	Wavenumber [cm ⁻¹]	x	Space dimension [m]
l	Angular momentum quantum number	Z	Nuclear charge number
L	Length [m]	y	Space dimension [m]

Greek

α	Internal angle crystal unit cell [°]	π	3.141...
β	Internal angle crystal unit cell [°]	π	Non-linear molecular orbital
γ	Internal angle crystal unit cell [°]	σ	Linear molecular orbital
ε	Absorption coefficient [m ² /mol]	φ	Azimuth angle [rad]
θ	Transmission angle after slit [rad]	ψ	Wavefunction [-]
ϑ	Polar angle [rad]	ω	Angular frequency [s ⁻¹]
λ	Wavelength [nm]		

Contents

Prologue	I
Summary	II
Samenvatting	III
Zusammenfassung	IV
Terminology	VI
1 Introduction	1
2 Theory	2
2.1 Structure of Rubrene	2
2.1.1 Molecular Orbital Theory	2
2.1.2 Structuring Rubrene	5
2.1.3 Crystal Structure	6
2.2 Spectroscopic Properties	7
2.2.1 Electronic Transitions	7
2.2.2 Absorption in Rubrene	8
2.2.3 Absorbance and Transmittance	9
2.3 Electron Diffraction	10
2.3.1 Electrons as a Wave	10
2.3.2 Diffraction of Light Waves	10
3 Methodology	14
3.1 Sample Preparation	14
3.2 Absorption Spectroscopy	16
3.2.1 Absorption Set-Up for Solid Crystallised Rubrene	16
3.2.2 Absorption Set-Up for Dissolved Rubrene	17
3.3 Electron Diffraction	18
4 Results	20
4.1 Prepared Samples	20
4.2 Absorption Spectroscopy	22
4.2.1 Absorption of Dissolved Rubrene	22
4.2.2 Absorption of Crystallised Rubrene	23
4.3 Electron Diffraction	25
4.3.1 Simulated Electron Diffraction Patterns	25
4.3.2 Practically Determined Electron Diffraction Patterns	29
5 Discussion	31
6 Conclusion	33
7 Outlook	35
8 Bibliography	36
Epilogue	38
Appendix A Hybridisation of Carbon Atoms	A
Appendix B Crystal Unit Cells	D
Appendix C Derivation of Diffraction	G

List of Figures

2.1	A ball-and-stick model of the structure formula of rubrene. As the legend suggests, the black balls represent carbon atoms whereas the white balls represent hydrogen atoms. Left: front view; Right: top view.	2
2.2	A schematic image of non-degenerate energy levels and atomic orbitals with the corresponding labels.	3
2.3	The atomic orbitals of importance. 2.3a shows the 90 percent representation of a s-orbital. 2.3b shows the 90 percent representation of a p-orbital. The aim of this section is to explain the construction of benzene and ultimately also that of rubrene. For that reason only the s- and p-orbitals are displayed. [2]	4
2.4	A 90 percent probability surface plot of the molecular π -orbital. The nodal plane also shown. This is the plane of zero amplitude, the probability that electrons are located on the nodal plane is also zero. An internuclear axis of a π -orbital is the axis at which the nuclei are positioned. [2]	5
2.5	Structuring a benzene rings with the molecular orbital theory. Each subfigure shows an important aspect of this and a corresponding explanation. [3]	5
2.6	An orthorhombic side-centred unit cell. The red circles represent a lattice, a (part of a) rubrene molecule.	6
2.7	Fig. 2.7a shows orientation A; Fig. 2.7b shows orientation B; Fig. 2.7c shows orientation C, where edge $a = 26.789 \text{ \AA}$, $b = 7.170 \text{ \AA}$, and $c = 14.211 \text{ \AA}$. The edge lengths are mentioned in the in the corresponding figures. Images extracted from CrystalMaker.	7
2.8	An example of electronic transitions for a bound molecule where the curve is the potential binding energy; the levels in the curve are the vibrational energy levels; and the sublevels are the rotational energy levels. [5]	8
2.9	This figure shows the electric field (black) and the intensity (blue) of a single slit diffraction situation.	11
2.10	The resulting electric field (Fig. 2.10a) and intensity (Fig. 2.10b) of multi beam interference for $N = 2, 4, 8$ Huygens waves.	12
2.11	The resulting electric field (Fig. 2.11a) and intensity (Fig. 2.11b) of multi slit diffraction for $N = 8$ slits. The values are not draws as they differ in each situation. . . .	12
3.1	Fig. 3.1a is a real image of a rubrene crystal on the tip of the yellow epoxy resin. Fig. 3.1b shows an illustration of the same situation with the corresponding measures. .	14
3.2	A photo and a sketch of the microtome with the knife and crystal.	15
3.3	On the top, one can see the rubrene crystal (orange). Bottom of the image is the diamond knife on which the lens system is focused.	15
3.4	Schematic representation of a transportation loop that nears a TEM mesh grid. [12]	15
3.5	The set-up of the absorption spectrometry for a crystallised sample slice. The set-up contains four parabolic concave mirrors which either collimate or focus the light. The light of the source is approximately a point source and contains UV- and/or Vis-light. The light is then focused on the sample slice. The remaining light, after absorption, transmission and scattering, will be directed to the spectrometer. Both the light source and the spectrometer are connected with optic fibre cables.	16
3.6	Two spectra of the used light source. The black spectrum represents the visible halogen light source whereas the blue spectrum represent the ultra violet deuterium light source.	17
3.7	Fig. 3.7a shows the blank measurement, the cuvette with pure chloroform (actually transparent). Fig. 3.7b shows the rubrene solution with the $c = 0.1, 0.05, 0.01 \text{ mmol/L}$	18
3.8	A schematic of the used diffractometer for the electron diffraction experiment. . . .	18
4.1	Rubrene sample cut at the thickness of $t = 250 \text{ nm}$. Fig. 4.1a and Fig. 4.1b depict the crystal probe A3. Fig. 4.1c and Fig. 4.1d depict the crystal probe B3. These pictures were taken with a ‘dark field imaging’ filter making the contrast of the image more pronounced.	20

4.2	Rubrene slices cut in different thicknesses and on different TEM grids. Fig. 4.2a and Fig. 4.2b depict a slice thickness of 140 nm on a 1500 Hexagonal TEM mesh grid. Fig. 4.2c and Fig. 4.2d depict a slice thickness of 100 nm on a 600 and thus courser Hexagonal TEM mesh grid.	21
4.3	Left (Fig. 4.3a), the absorption spectrum in UV-Vis spectrum range; right (Fig. 4.3b), the absorption spectrum in Vis-range. Both contain the spectra of the concentrations $c = 0.1, 0.05, 0.01$ mmol/L dissolved in chloroform. In Fig. 4.3b, the absorption peaks, which are numbered from low to high energies, are also indicated.	22
4.4	The absorption spectra of two crystals at thickness $t = 250, 200, 150$ nm. These measurements are conducted with unpolarised light. A Gaußian data smoother is used to present the spectra.	23
4.5	Absorption as a function of the wavelength where the polarisation of the light is rotated. Crystal A3 is used for this measurement, cut at $t = 120$ nm, and placed on a 1500 hexagonal mesh. A Gaußian data smoother is used to present the spectra. .	24
4.6	Simulated diffraction pattern of rubrene crystal on orientation A, Fig. 2.7a. The horizontal and vertical axis of the image represent the pixels, which are square in the image. Note that the used colour scale is linear. Figure extracted from CrystalMaker and SingleCrystal.	25
4.7	The plotted intensities of the zeroth and first order vertical line of crystal orientation A.	26
4.8	Simulated diffraction pattern of rubrene crystal on orientation B, Fig. 2.7b. The horizontal and vertical axis of the image represent the pixels, which are square in the image. Note that the used colour scale is linear. Figure extracted from CrystalMaker and SingleCrystal.	26
4.9	The zeroth order horizontal and vertical line of crystal orientation B.	27
4.10	Simulated diffraction pattern of rubrene crystal on orientation C, Fig. 2.7c. The horizontal and vertical axis of the image represent the pixels, which are square in the image. Note that the used colour scale is linear. Figure extracted from CrystalMaker and SingleCrystal.	27
4.11	The zeroth and first order horizontal line of crystal orientation C.	28
4.12	An example of the electron beam that is focused on a sample. Images taken with an exposure time of one second.	29
4.13	Left: electron diffraction of crystal A3 at $U = 35$ kV and an effective exposure time of 300 s. Note that both axis contain pixel counts on equal axis, and that the colour scale is logarithmic. Right: rotated simulated electron diffraction result of orientation A to support visual comparison.	29
4.14	Left: electron diffraction of crystal B1 at $U = 35$ kV and an effective exposure time of 300 s. Note that both axis contain pixel counts on equal axis, and that the colour scale is logarithmic. Right: rotated simulated electron diffraction result of orientation C to support visual comparison.	30
5.1	Molecular unit in crystal orientation A.	32
A.1	A schematic representation of the electron configuration according to valence bond theory.	A
A.2	The electron configuration of a sp^3 -hybridised carbon atom. Here can be seen that two s-electrons have been promoted to sp-electrons and that two p-electrons have been demoted to sp-electrons.	A
A.3	This figure depicts a sp^3 -hybridised carbon atom. The black lines represent the sp-orbital which is illustrated for the vertical orbital. [2]	B
A.4	The electron configuration of a sp^2 -hybridised carbon atom. Here can be seen that two s-electrons have been promoted to sp-electrons and that only one p-electrons has been demoted to sp-electrons. The last p-electron remains in its original state.	B
A.5	This figure depicts a sp^3 -hybridised carbon atom. The black lines represent the sp-orbital, whereas the yellow shapes represents the p-orbital. [2]	B
A.6	The electron configuration of a sp-hybridised carbon atom. Here can be seen that two s-electrons have been promoted to sp-electrons and that no p-electrons have been demoted to sp-electrons. The p-electrons remain in their original state.	C

A.7	This figure depicts the bonds of an ethyne molecule where the carbon atoms are sp-hybridised. The black lines still represent the sp-orbital that don't bind to the carbon, whereas the yellow shapes represents the π -bonds and σ -bond of the carbon atoms. [2]	C
B.1	Three possibilities of cubic latticed unit cells.	D
B.2	Two possibilities of tetragonal latticed unit cells.	D
B.3	Four possibilities of orthorhombic latticed unit cells.	E
B.4	Two possibilities of monoclinic latticed unit cells	E
B.5	The triclinic latticed unit cell.	F
B.6	The hexagonal latticed unit cell.	F
C.1	An illustration of a single slit experiment with light.	G
C.2	The electric field continuously shifts phase resulting in interference. Sometimes constructively, sometimes destructively. Fig. C.2a represents destructive interference as there is no electric field vector. Fig. C.2b represents constructive interference as the image shows the largest electric field possible. [23]	H
C.3	A part of a phasor diagram where E_0 is the total continuous electric field. [23] . .	I
C.4	A normalised example of the sinc function for the electric field (the blue graph) and the sinc function squared for the intensity (the orange graph). Note that the electric field can reach below zero which would never be possible for the intensity as intensity must be greater than zero. The intensity only shows positive maxima and minima which equal zero.	J
C.5	The resulting electric field (Fig. C.5a) and intensity (Fig. C.5b) of multi beam interference for $N = 2, 4, 8$ Huygens waves.	K
C.6	The resulting electric field (Fig. C.6a) and intensity (Fig. C.6b) of multi slit diffraction for $N = 8$ slits. The values are not draws as they differ in each situation. . . .	L

List of Tables

2.1	An overview of the possible unit cells in a crystal with the corresponding edge lengths and internal angles. As the values of the lengths and some angles differs per crystal, a more algebraic notation is used. [4]	6
2.2	Values of the edge lengths and the internal angles of the rubrene orthorhombic side-centred unit cell.	7
4.1	Peak absorption wavelengths with corresponding wavenumbers.	22
4.2	Absorption coefficients at the peak wavelength for the rubrene concentration $c = 0.1$ mmol/L.	23
4.3	The wavelengths and wavenumbers of the absorption spectra shown in Fig. 4.4. The absorption peaks are listed from low to high energies.	24
4.4	A summary of the simulated results per orientation. The first second column shows the results from the diffraction images; the fourth column shows the results from the known edge lengths of the crystal's unit cell.	28
B.1	An overview of the possible unit cells in a crystal with the corresponding edge lengths and internal angles.	D

1 Introduction

Organic molecules have specific spectroscopic properties: absorption wavelengths and emission wavelengths. By crystallising organic molecules, one combines their spectroscopic properties with the macroscopic functionality of condensed matter (such as semi-conduction). These organic molecular crystals are highly interesting materials to study. The most fundamental processes for electro-optical applications are the interaction of light with molecules and the propagation of charges and energy within the crystal. This can have useful applications in photovoltaics and organic light emitting diodes (OLED). In photovoltaics, light is absorbed by molecules in a crystal. This can happen if the energy is equal to or higher than the energy bandgap. Then, the electrons will be able to move freely throughout the crystal. Oppositely, a voltage can be applied which causes electrons of the molecule to propagate, leaving a hole. Electrons from the external voltage source can then fill up the holes to create an exciton and emit light.

Within the Max Planck Institute for the Structure and Dynamics of Matter, a research is commencing to investigate the behaviour of organic crystals at various temperatures ranging from room temperature down to approximately 10 K. For this, the electronic states of the molecules in the crystals are excited with a pump-probe set-up. The excitation will be done with ultrashort laser pulses with a pulse duration of approximately 30 fs. This is due to the relevant motion of electrons happening on the femtosecond timescale. Matter in excited state contains more energy than matter in the ground state. Other molecular orbitals will be occupied which has a changing effect on the structure and electro-optical properties of the molecule. In the pump-probe set-up, a specific time is awaited for the excited system to relax before the response of that system is probed by either an ultrashort laser pulse for Transient Absorption Spectroscopy (TAS) or an electron pulse for Ultrafast Electron Diffraction (UED). TAS will be conducted to measure the change in absorption due to electrons already being in a higher energetic state which cannot absorb the same wavelength again. UED will be conducted to measure the change in structure. In short, TAS is applied to investigate the electro-optical changes of the crystal; UED is applied to investigate the structural changes of the crystal.

Before TAS and UED experiments can be conducted, characterisation of the crystal's ground state is needed. In this project, the crystal in question is an organic molecular crystal, rubrene. The spectroscopic properties is studied by conducting absorption spectroscopy experiments; the structure of the ground state crystal is investigated using electron diffraction. The former gives useful information about the crystal's absorption wavelengths, which is also needed to determine the most efficient excitation wavelength for the crystal. The absorption spectra of rubrene is measured using both polarised and unpolarised light for the crystallised sample as the crystal is anisotropic. Furthermore, the absorption of dissolved rubrene is also measured which is polarisation independent. Electron diffraction gives information about the structure of the crystal and its crystal orientation, and it will become clear whether the crystal is unharmed by the method of sample preparation.

The penetration depth of light and electrons is roughly a few hundred nanometres in rubrene. The crystal must therefore be cut into very thin slices of tens to hundreds of nanometres. This is done by using an ultramicrotome. The ultramicrotome is a machine used to cut samples very thinly. The sample will be attached to the microtome's arm which rotates back and forth, and, when nearing the sample, translates vertically down cutting a sample slice.

In the next chapter, the theoretical background of the project is discussed in order to better understand the methodology and results. Next is the methodology where the preparation of the experiments and the actual conducted experiments are explained along with their experimental set-ups. After the methodology, the results of the conducted experiments are presented, clarified, and substantiated. In the fifth chapter, the methodology of the experiments and the obtained results will be discussed on their accuracy, validity, and reliability. In the sixth chapter, conclusions will be drawn based on the results and discussion. Lastly, an outlook of the research's future will be offered.

2 Theory

In the theory chapter, the necessary theory will be explained in order to understand the overall research and methodology and results. Firstly, the structure of rubrene will be discussed in detail, containing molecular orbital theory and then the crystallography of the rubrene crystal. Secondly, the physics of absorption spectroscopy is explained, containing the energy states on a molecular scale and the macroscopic Beer-Lambert law. Combined, they explain the absorption of rubrene. Lastly, electron diffraction is discussed, explaining how an electron can act as a wave and interfere creating diffraction. Further, general diffraction is discussed.

2.1 Structure of Rubrene

Rubrene, $C_{42}H_{28}$, is an organic molecule. Organic molecules contain carbon bindings similar to molecules created by organisms. Rubrene is constructed from eight benzene rings, a widely used organic molecule itself. In principle, benzene is a hexagon of carbon atoms with additional hydrogen atoms. To even explain how a benzene ring is constructed, more knowledge about the covalent bindings and molecular orbital theory that is the absolute foundation of this topic is necessary. But first, Fig. 2.1 shows the ‘classic’ structure formula of rubrene.

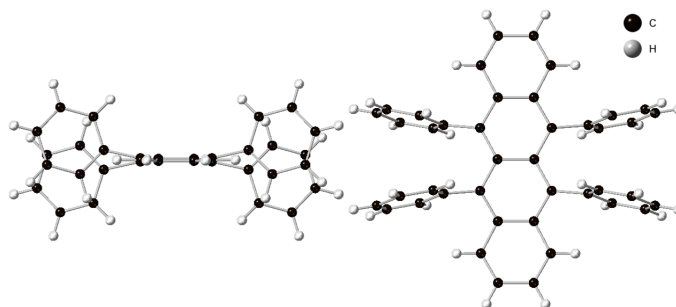


Figure 2.1: A ball-and-stick model of the structure formula of rubrene. As the legend suggests, the black balls represent carbon atoms whereas the white balls represent hydrogen atoms. Left: front view; Right: top view.

This paragraph aims to explain how this molecule and crystal is constructed from a physical perspective.

2.1.1 Molecular Orbital Theory

In this subparagraph, the theory of molecular orbital theory will be explained shortly to obtain an understanding of the matter and get a sense of the emanating results.

Molecular orbital theory describes the formation of molecular orbitals from a combination of atomic orbitals. An atomic orbital is a direct results of quantum mechanics and a solution of the Schrödinger equation. So, to explain molecular orbitals, atomic orbitals first have to be discussed. The time independent, one dimensional, non-relativistic Schrödinger equation predicts stationary states of the wave function and is given by:

$$-\frac{\hbar^2}{2m} \frac{d^2\psi}{dx^2} + V\psi(x) = E\psi(x). \quad (2.1)$$

In this equation $\hbar = \frac{h}{2\pi} = 1.0546 \cdot 10^{-34}$ [J·s] is Dirac’s constant, m is the mass of the particle in question, $\psi(x)$ is the wave function, x is the one dimensional direction variable, V is the potential energy, and E is the total energy of the considered system. The wave function squared $\psi(x)^2$ represents the probability of a particle’s location.

The equation can be written for a single electron orbiting a single proton, i.e. the system of a hydrogen atom. For this, the primitive of Coulomb’s law is substituted for the potential energy,

and is Bohr's model used to express the energy level. Naturally, this must not be solved in one dimension but in three. The simplest way to solve the wave function would be by using spherical coordinates.

A three dimensional solution does not only give restriction to certain energy states, but orbital shapes also. These restrictions are a result of the three dimensional Schrödinger equation where three parameters emerge as indices. The three quantum numbers that emerge from the solutions and their allowed values are:

n	principle quantum number	$1, 2, 3, \dots, n$
l	angular momentum quantum number	$0, 1, 2, \dots, n - 1$
m_l	magnetic quantum number	$0, \pm 1, \pm 2, \dots, \pm l$

The principle quantum number n describes effectively the electron shells that appear in Bohr's model of the atom: K-, L-, and M-shell. So, the higher the principle quantum number, the higher the energy level, a phenomenon that is rather well described by Bohr's model. However, it would only be correct for hydrogen-like atoms. Later more about this specific topic. The angular momentum quantum number l describes subshells of each electron shell. This partly determines the amount of electrons able to occupy an energy level. The magnetic quantum number m_l better specifies the subshells and determines the amount of electrons that are allowed to occupy the subshell. There is one other quantum number that should be considered: the magnetic spin quantum number m_s . Electrons can assume a spin value of $\pm \frac{1}{2}$.

Pauli's exclusion principle states: "*No two electrons in a single atom can have the same set of quantum numbers (n, l, m_l, m_s) [1].*" This means that every electron in an atom *must* have different quantum numbers which has interesting consequences.

As mentioned, the principle quantum number describes the energy levels of electrons in an atom. However, one could imagine when there are numerous electrons on the same energy level (e.g. $n = 2$) that this causes Coulomb interactions between electrons. Consequently, electrons will be a little repelled outwards. Meaning that an electron (in a multiple electron atom) experiences an effective nuclear charge that is less than the actual nuclear charge. This phenomenon is described by the shielding effect, or electron shielding.

So, instead of subshells being degenerate the higher subshells, $> l$ -values, will have a higher energy and therefore be bound more weakly. This is, however, only true for non hydrogen-like atoms. In Fig. 2.2 a schematic image of non-degenerate energy levels of atomic orbitals is given.

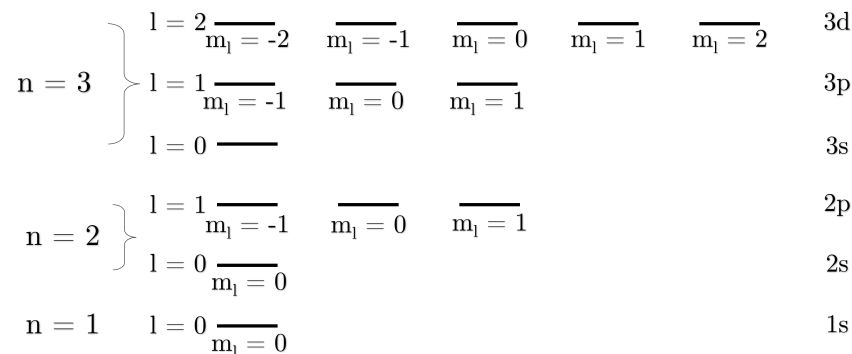


Figure 2.2: A schematic image of non-degenerate energy levels and atomic orbitals with the corresponding labels.

Each electron quantum state has a certain 'shape', actually a probability at which an electron is located, the atomic orbital. An atomic orbital can be occupied by one or two electrons, paired and

unpaired, respectively. Paired electrons must still follow Pauli's exclusion principle, so they must have opposite spin.

The ground state of an atom is the situation where the atomic orbitals are occupied systematically in order to obtain the most energetically favourable state. This is also described by Hund's maximum multiplicity rule which states: "*An atom in its ground state adopts a configuration with the greatest number of unpaired atoms* [2]." Meaning, electrons will remain unpaired for as long as possible and will occupy the degenerate orbitals first. The order of occupying atomic orbitals is determined by the electron configuration. The electron configuration of several atoms:

H:	$1s^1$	C:	$[\text{He}]2s^2 2p^2$
He:	$1s^2$	N:	$[\text{He}]2s^2 2p^3$
Li:	$1s^2 2s^1$ or $[\text{He}]2s^1$	O:	$[\text{He}]2s^2 2p^4$

The superscript on the orbital letters shows how many electrons occupy the particular atomic orbital. Not every orbital contains paired electrons, with exception to noble gasses, and only the unpaired electrons are able to bind to an orbital of another atom. How this could be possible is quite simple. The location of an electron is given by a probability wave function, a solution of the Schrödinger equation. These are the atomic orbitals which are commonly represented by a 90 percent probability plot. Meaning, there is a 90 percent probability an electron is located within the plotted region. In Fig. 2.3 the s-orbital, Fig. 2.3a, and the p-orbital, Fig. 2.3b are shown.

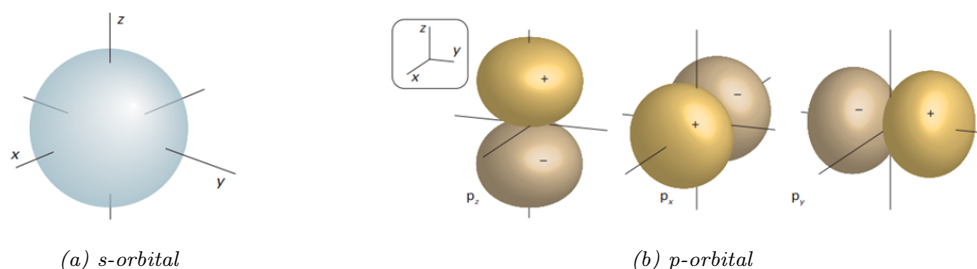


Figure 2.3: The atomic orbitals of importance. 2.3a shows the 90 percent representation of a s-orbital. 2.3b shows the 90 percent representation of a p-orbital. The aim of this section is to explain the construction of benzene and ultimately also that of rubrene. For that reason only the s- and p-orbitals are displayed. [2]

When two wave functions (atomic orbitals) interfere they can either interfere constructively or destructively. For simplicity's sake, only constructive interference is considered. Constructive interference will cause the wave function to 'fuse' and form a bond. Both electrons then share a location probability and could possibly both be orbiting one atom or could both be at a different atom.

Hydrogen atoms, for example, ($1s^1$) would bind linearly for it would not matter where the bond would be, it will always be linear. The linear bond, or linear molecular orbital, between two atoms is named after the s-orbital, the σ -bond (for the Greek letter 's'.) p-orbitals have two ways of bonding: linearly and non-linearly. A linear bond between two p-orbitals or a p- and a s-orbital is still a σ -orbital. That would only be possible in three distinctive directions, but p-orbitals are also able to bind non-linearly by creating a bridge-like structure. The non-linear bond between atoms is named after the p-orbital, the π -orbital (for the Greek letter 'p').

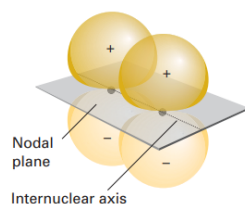


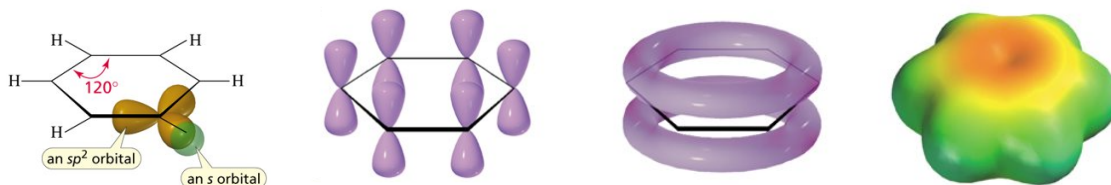
Figure 2.4: A 90 percent probability surface plot of the molecular π -orbital. The nodal plane also shown. This is the plane of zero amplitude, the probability that electrons are located on the nodal plane is also zero. An internuclear axis of a π -orbital is the axis at which the nuclei are positioned. [2]

Returning to atoms and the application of the orbitals, one might see an inconsistency. Carbon, $[\text{He}]2s^22p^2$, merely contains two unpaired electrons, yet it is widely known carbon is able to have four covalent bonds. According to this model, the valence bond theory, carbon would not be able to do that.

To resolve this issue the model must be extended to molecular orbital theory. Molecular orbital theory takes more variables into account such as charge repulsion and more energetically favourable states. The consequence for carbon would be that electrons are promoted and demoted and causes orbitals to hybridise. Naturally, electrons in carbon atoms are not actually promoted to a higher energy state, it would rather be the solution of the wave function when more variables are considered [2]. Carbon hybridisation is explained in Appendix A for further reading.

2.1.2 Structuring Rubrene

Carbon in benzene rings is sp^2 -hybridised. Meaning, two s-electrons are promoted, one p-electron is demoted, and one p-electron remains unchanged. This enables carbon atoms to bind twice to the same atom with a σ - and π -orbital. Because the sp -orbitals are 120° rotated respectively to each other, they are able to bind hexagonally (the internal angle of a hexagon is 120°).



(a) Every carbon atom in a benzene ring has three sp^2 -orbitals. One of them is illustrated sharing a σ -bond with a hydrogen atom. (b) Also every carbon atom in a benzene ring has a vertically orientated p-orbital. All of them are illustrated in the image. (c) The p-orbitals all interfere constructively and form a ring. So they all share six electrons in the big π -orbital. (d) A more accurate representation is shown here. The illustration shows the electron density of benzene (green high, orange low).

Figure 2.5: Structuring a benzene rings with the molecular orbital theory. Each subfigure shows an important aspect of this and a corresponding explanation. [3]

Now that the structure of benzene is clear and discussed, let's expand this model to multiple benzene rings until rubrene is obtained. As is discussed, every carbon atom in benzene binds twice to other carbon atoms and once to hydrogen. Imagine an extra benzene ring comes along and takes away two of those hydrogen atoms and two of the carbon atoms and binds to the benzene, creating naphthalene (two benzene rings connected at the long edge). This would mean that the binding's original σ -bonds with hydrogen would be replaced with σ -bonds with carbon. Also, the π -bonds of the benzene rings would interfere constructively and fuse. One can do this a couple of times until four benzene rings are connected creating tetracene. Then four other benzene rings are connected, rotated 90° from the horizontal plane, two on the second ring and the other two on the third ring, like Fig. 2.1. This connection is actually a linear σ -bond between two carbon atoms with one of

their sp-hybridised orbitals. Logically, the side rings are not part of the fused π -orbitals of the tetracene, but only interfere internally in the benzene compound.

2.1.3 Crystal Structure

There are numerous ways to structure a crystal with several types of bonds: metallic bond, ionic bond, covalent bond and van der Waals bond. Rubrene forms a crystal structure with itself by using van der Waals bonds, the weakest bond. Consequently, the crystal is fragile. A van der Waals force acts up with dipole molecules. This is the case with rubrene where the carbon atoms attract the electrons more due to the heavier nucleus than hydrogen's.

A crystal is commonly expressed and represented in unit cells which can be regarded as a fundamental 'building block' of crystals with edge lengths a , b , and c and corresponding angles α , β , and γ of which an example is shown in Fig. 2.6. Unit cells are classified into seven crystal systems by noting the rotational symmetry they possess. Tab. 2.1 summarises all possible unit cells along with their edge and angle identities.

Table 2.1: An overview of the possible unit cells in a crystal with the corresponding edge lengths and internal angles. As the values of the lengths and some angles differs per crystal, a more algebraic notation is used. [4]

Unit cells	Edge lengths	Internal angles
Cubic	$a = b = c$	$\alpha = \beta = \gamma = 90^\circ$
Tetragonal	$a = b \neq c$	$\alpha = \beta = \gamma = 90^\circ$
Orthorhombic	$a \neq b \neq c$	$\alpha = \beta = \gamma = 90^\circ$
Monoclinic	$a \neq b \neq c$	$\alpha = \beta = 90^\circ \neq \gamma$
Trigonal	$a \neq b \neq c$	$\alpha \neq \beta \neq \gamma \neq 90^\circ$
Hexagonal	$a = b \neq c$	$\alpha = \beta = 90^\circ \neq \gamma = 120^\circ$
Triclinic	$a \neq b \neq c$	$\alpha \neq \beta \neq \gamma \neq 90^\circ$

Within these categories there are also sub-group unit cells: primitive, body-centred, face-centred, and side-centred (or end-centred) unit cell. Including the sub-groups, there are 14 distinct space lattices, Appendix B discusses this specific topic in more detail while this paragraph focuses on the crystal structure at hand.

Rubrene can be crystallised in an orthorhombic side-centred crystal lattice. So, the unit cell's edges are not equal, but the internal angles are, which makes it a cuboid. Side-centred merely means that extra lattices are present at the top and bottom plane of the unit cell. In Fig. 2.6 a schematic illustration of such unit cell is presented.

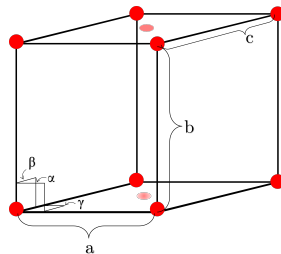


Figure 2.6: An orthorhombic side-centred unit cell. The red circles represent a lattice, a (part of a) rubrene molecule.

Values of the rubrene orthorhombic side-centred unit cell are specified in Tab. 2.2.

Table 2.2: Values of the edge lengths and the internal angles of the rubrene orthorhombic side-centred unit cell.

Edge Lengths		Internal angles	
a	26.789 Å	α	90°
b	7.170 Å	β	90°
c	14.211 Å	γ	90°

Orientation plane A is defined with the edge lengths b and c , so the front view; orientation B is defined with edge lengths a and c , the side view; orientation C is defined with edge lengths a and b , top view. The orientations of the orthorhombic side-centred unit cell from CrystalMaker, a crystal simulator, are depicted in Fig. 2.7 with appropriate dimensions in Angstrom.

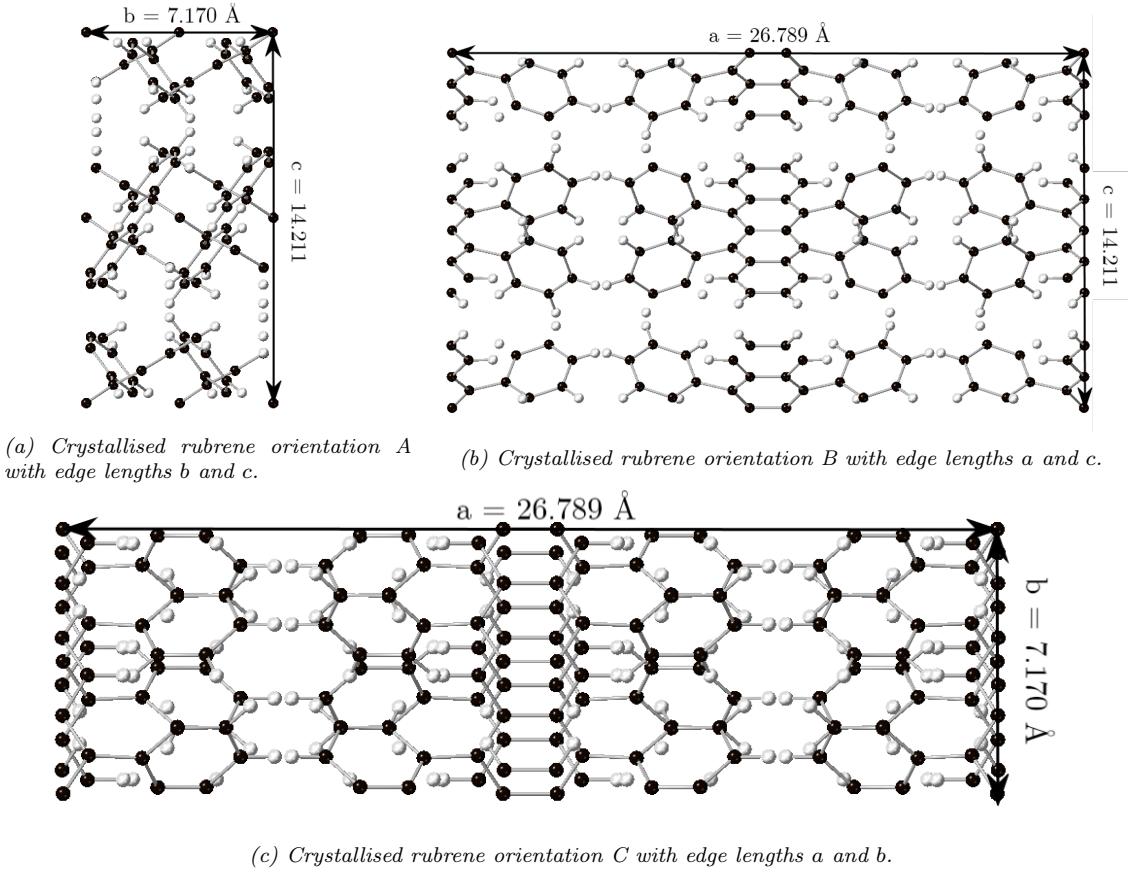


Figure 2.7: Fig. 2.7a shows orientation A; Fig. 2.7b shows orientation B; Fig. 2.7c shows orientation C, where edge $a = 26.789$ Å, $b = 7.170$ Å, and $c = 14.211$ Å. The edge lengths are mentioned in the in the corresponding figures. Images extracted from CrystalMaker.

2.2 Spectroscopic Properties

Spectroscopy is a term for measuring a spectrum, it includes various types of spectroscopy such as rotation and vibration spectroscopy. This paragraph will mainly focus on absorption spectroscopy in the UV-Vis (i.e. Ultra Violet and Visible spectrum) and electronic transition to further explain the absorption properties of rubrene.

2.2.1 Electronic Transitions

A step back to the atomic model of electronic transitions: when an electron is excited to a higher energy state, it will fall back to the ground state to reach its most energetically favourable equilibrium. When losing this newly obtained potential energy, the law of conservation of energy must

still be obeyed. Resulting in photon emittance exactly equal to the lost potential energy.

Although this is a highly simplified model, its fundamental physics is still valid. A more realistic model of electron transitions in polyatomic molecules is similar to Fig. 2.8. This figure shows more complex behaviour of electronic transitions and explains why the emitted photon is not of equal wavelength as the absorbed photon. Also, in Fig. 2.8, the vibrational and rotational levels are depicted.

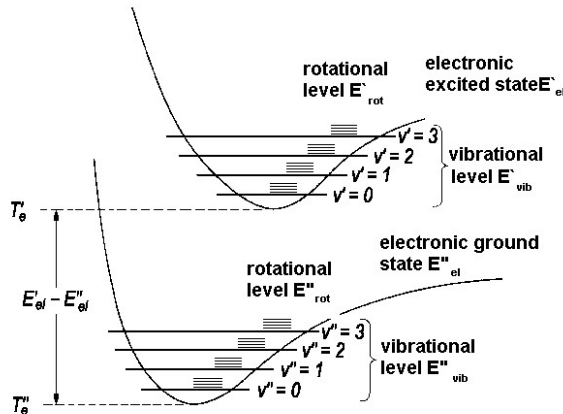


Figure 2.8: An example of electronic transitions for a bound molecule where the curve is the potential binding energy; the levels in the curve are the vibrational energy levels; and the sublevels are the rotational energy levels. [5]

The curved graphs drawn in the picture represent the potential energy curve in which the electron is ‘trapped’. In this potential, more energy states are available: vibrational levels. Moreover, on each vibrational level are rotational energy levels. These sub-energy levels also result from quantum mechanics. The absorption of a photon follows the Franck-Condon principle which states: “*Because the nuclei are so much more massive than the electrons, an electronic transition takes place very much faster than the nuclei can respond* [6].” Meaning, absorption of a photon is represented by a vertically rising line due to the slow reaction of the nuclei. Imagine the ground state, with vibration and rotation level zero, is excited to the next molecular orbital. It cannot, however, be excited to the ground state of the next molecular orbital, because the probability is extremely low. It will rather be excited a little higher, several vibrational levels on top of the potential energy. As this is quantum mechanics, the model and reality still has to account for the probability that an electron is excited to various vibrational levels. Vibrational levels are separated periodically, following [6]:

$$E_{vib} = \left(n + \frac{1}{2}\right) \hbar\omega, \quad (2.2)$$

indicating several absorption levels to which an electron can be excited. One would also expect to see some periodicity in the absorption spectrum.

2.2.2 Absorption in Rubrene

The electronic transition at hand is the HOMO – LUMO (Highest Occupied Molecules Orbital – Lowest Unoccupied Molecular Orbital) transition, and in this case $\pi \leftarrow \pi^*$ (“pi to pi star transition”). This transition is typically in UV-Vis spectral range. Remember the rubrene molecule: a tetracene compound base with four separate benzene compound rotated 90° attached on the sides of two centred carbon circles. The attached benzene absorbs in UV, the tetracene compound absorbs in the visible spectrum. This can easily be explained by a simplified model of the fused π -orbitals. The π -electrons are bound to the molecule due to the binding potential. By assuming the potential is infinite, the model of particle in a box can be applied [7]. The length of a particle in a box is an important variable for the resulting energy levels: the larger the orbital lengths, the larger the

wavelength, and thus the smaller the energy difference between energy states. Energy states of this particle in a box simplification is described by the following relation:

$$E_n \propto \frac{1}{\lambda_n} \propto \frac{1}{L^2}, \quad (2.3)$$

where E_n is the energy level of the particle in the box, the electron, λ_n the corresponding wavelength (following the Broglie relation), and L the length of the box in the simplified model, or the length of the π -orbital.

If more benzene rings bind together and fuse their π -orbitals, the length of the particle in a box L will increase accordingly, resulting in a lower energy difference E_n . Due to a lower energy difference, a larger wavelength λ light is capable to excite electrons to a higher molecular orbital causing the absorption to shift from UV to visible light when connecting more benzene compounds to the centre molecule.

Rubrene is a molecule that contains tetracene as well as benzene compounds implying that rubrene would absorb in UV and visible light. When assuming the tetracene compound is orientated on the horizontal plane, then the benzene compounds of rubrene must be orientated on the vertical plane (see Fig. 2.1). Regardless of the compound's orientation, with unpolarised light, one would measure all absorption peaks. However, when one does use linearly polarised light for spectroscopic measurements on crystallised rubrene, some peaks will likely vanish on certain rotational angles. This is due to the vibration orientation of linearly polarised light and the orientation of the rubrene molecules in the crystal structure. When the light is vibrating parallelly to the organic compound's orientation plane, the probability of absorption would be significantly less. On the other hand, if the light vibrates perpendicular to the organic compounds, the probability of absorption will significantly increase.

This is only true for solid state spectroscopy, it is untrue for solution based spectroscopy, though. In a solution, rubrene would be evenly distributed and orientated in practically every orientation which makes polarised light an unusable feature in solvent based spectroscopy. Besides, rubrene is dissolved in a liquid which results in a smaller chance of interaction between the rubrene molecules. Less interaction between the rubrene molecules gives blueshifted absorption peaks compared to crystallised absorption. Due to interaction between neighbouring rubrene molecules, such as in a crystallised solid, the energy levels decrease slightly making the absorption peaks redshifted. This is called the 'crystal shift'.

2.2.3 Absorbance and Transmittance

When a broad spectrum of light is shone upon a substrate some of the light will be transmitted, some of the light will be reflected or scattered, and some of the light will be absorbed. Only transmission and absorption will be considered for now. Light is commonly measured by its intensities which is proportional to the square of its electric field. The Beer-Lambert law describes the relation between the incoming light and the exiting light, it is expressed as [6]:

$$I = I_0 10^{-\varepsilon c L}, \quad (2.4)$$

where I is the light intensity after the absorption and transmission in Watt per surface unit [W/m^2]; I_0 the intensity before the sample also in [W/m^2]; ε the absorption coefficient in [m^2/mol] or [$\text{M}^{-1}\text{cm}^{-1}$]; c the concentration of the sample in [mol/m^3] or [M] and L the length of the sample in metres [m].

The amount of transmitted light is intuitively given by the transmittance and is expressed as the measured intensity over the incoming intensity [6]:

$$T = \frac{I}{I_0}, \quad (2.5)$$

where T is the transmittance which is unitless, but merely a measure of the amount of transmitted light. Consequently, the value of the transmittance will be $0 < T < 1$. The absorbance on the other hand is the tenth logarithm of the inverse of the transmittance [6]:

$$A = \log_{10} \left(\frac{I_0}{I} \right) = -\log_{10}(T) = \varepsilon cL. \quad (2.6)$$

Although A is unitless, it is often expressed in optical density [OD], a logarithmic measure of absorbed light.

2.3 Electron Diffraction

Wave interference plays a huge role in diffraction, and can also explain the periodically changing minima and maxima. In this paragraph, the wave-particle duality will be introduced to explain why electrons can interfere and thus diffract. Next, general diffraction (of electromagnetic waves) shall be discussed, but will later return to the application on electron diffraction.

2.3.1 Electrons as a Wave

The threshold to quantum mechanics is the wave-particle duality. Every particle or wave behaves as a wave or particle, respectively, simultaneously. Electromagnetic waves is a great example of the latter: its particle is called a photon. That's why electron particles also behaves as waves. This phenomenon is described by the Broglie relation:

$$\lambda = \frac{h}{p} = \frac{h}{mv}, \quad (2.7)$$

indicating that a particle with a velocity v and mass m results in a wavelength λ . Oppositely, a wave with wavelength λ has a momentum p . With sufficient speed an electron can have a wavelength in the order of picometres. Light with such wavelength is known as X-rays. If electrons at high speed act like waves, they must also be able to interfere, and thus diffract. If a high energy electron is aimed at a sample such as rubrene and traverses, it will interact with the molecules of the crystal and therefore be scattered. The electrons will interfere constructively and destructively and create a diffraction pattern. That pattern cannot be detected directly, but must be observed indirectly by using a phosphorescent plate which will light up when the diffracted high energy electron collide with it. These diffraction patterns can then be detected and analysed.

Moreover, the scattering of electrons is not solely dependent on the structure of rubrene, also the charge of the atoms plays a huge role. One can imagine an atom with a large nucleus (high Z) will interact more strongly with an electron than an atom with a smaller nucleus. Rubrene contains carbon and hydrogen atoms: $Z_C = 6$ and $Z_H = 1$, which makes it a poor scatterer. The rubrene crystal will still scatter nonetheless.

2.3.2 Diffraction of Light Waves

Diffraction can be achieved with all kinds of waves: electromagnetic, acoustic, electrons, neutrons etc.. Because the principle of diffraction of all is similar, merely general diffraction for light waves will be explained in this section.

Diffraction can roughly be separated in two categories: Fraunhofer and Fresnel diffraction. In short, Fresnel diffraction is applicable in most cases regardless of the incoming light and optical path length, whilst Fraunhofer diffraction is an approximation where the incident wave is a plane wave and where the outgoing wave can also be considered a plane wave. As the Fraunhofer approximation will be used in the experiment, this will also be discussed here.

When light is transmitted through an infinitesimal hole, the outgoing light will be a half a sphere of a point source due to Huygens' Principle. This model allows one to regard a slit as infinite

adjacent holes without spaces in between, or infinite Huygens waves exiting the slit. Multiple Huygens waves will not merely exit the slit, but interfere with one another due to an introduced phase difference [8, 9]. In Appendix C, the derivation of single slit diffraction, multi beam interference and multi slit diffraction is shown. The electric field and intensity of single slit diffraction is given by:

$$E(\theta) = E_0 \frac{\sin\left(\frac{\pi}{\lambda} b \sin(\theta)\right)}{\frac{\pi}{\lambda} b \sin(\theta)}, \quad (2.8)$$

and

$$I(\theta) = I_0 \left(\frac{\sin\left(\frac{\pi}{\lambda} b \sin(\theta)\right)}{\frac{\pi}{\lambda} b \sin(\theta)} \right)^2. \quad (2.9)$$

One can recognise Eq. 2.8 as the sinc (sine cardinal) function ($\text{sinc}(x) = \frac{\sin(x)}{x}$), and, consequently, Eq. 2.9 as the sinc function squared. When plotting the intensity, one can clearly see maxima and minima, see Fig. 2.10. The maxima are the constructive interferences of the diffraction pattern whilst the minima are the destructive interferences of the diffraction pattern. By analysing these patterns, one can learn something about the slit's width, for example.

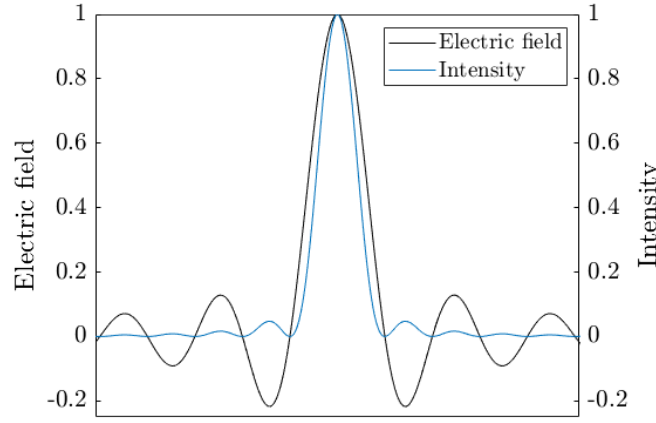


Figure 2.9: This figure shows the electric field (black) and the intensity (blue) of a single slit diffraction situation.

However, electron diffraction on rubrene the single slit model is not applicable, but an N-slit model must be applied. To expand this problem, one must first understand multi beam interference, see Appendix C. The electric field and intensity of multi beam interference is given by:

$$E(\theta) = E_0 \frac{\sin\left(\frac{N\pi}{\lambda} s \sin(\theta)\right)}{\sin\left(\frac{\pi}{\lambda} s \sin(\theta)\right)}, \quad (2.10)$$

$$I(\theta) = I_0 \left(\frac{\sin\left(\frac{N\pi}{\lambda} s \sin(\theta)\right)}{\sin\left(\frac{\pi}{\lambda} s \sin(\theta)\right)} \right)^2. \quad (2.11)$$

As can be seen, a new variable s is introduced. This is the distance between slits and influences the location of the maxima. Besides, the denominator of Eq. 2.10 and Eq. 2.11 contains a new parameter N which represents the total amount of Huygens waves. These function are plotted in Fig. 2.10 for $N = 2, 4, 8$ slits.

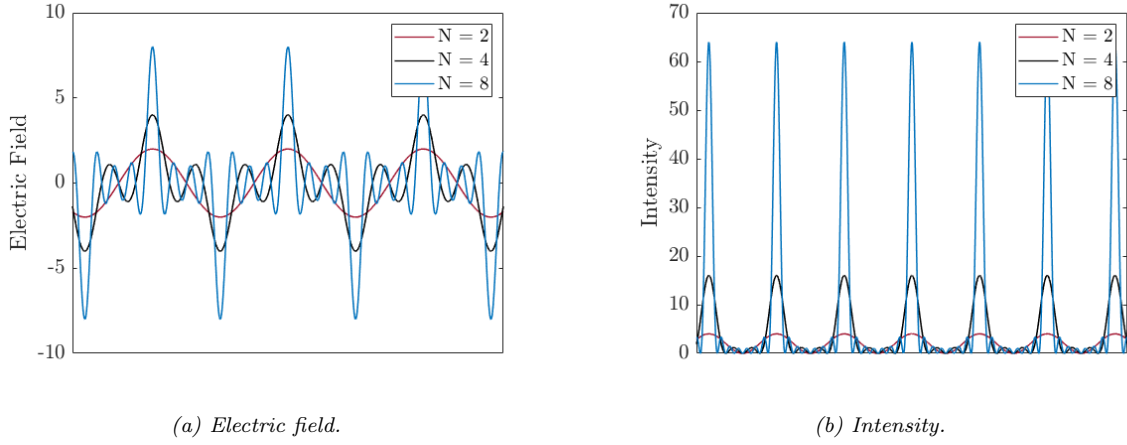


Figure 2.10: The resulting electric field (Fig. 2.10a) and intensity (Fig. 2.10b) of multi beam interference for $N = 2, 4, 8$ Huygens waves.

Now, expanding the model to multi slit diffraction one merely has to multiply Eq. 2.8 and Eq. 2.10 (excluding the amplitudes) to obtain an expression for the electric field, idem dito for Eq. 2.9 and Eq. 2.11 for the intensity.

$$E(\theta) = E_0 \frac{\sin\left(\frac{\pi}{\lambda} b \sin(\theta)\right)}{\frac{\pi}{\lambda} b \sin(\theta)} \frac{\sin\left(\frac{N\pi}{\lambda} s \sin(\theta)\right)}{\sin\left(\frac{\pi}{\lambda} s \sin(\theta)\right)} \quad (2.12)$$

$$I(\theta) = I_0 \left(\frac{\sin\left(\frac{\pi}{\lambda} b \sin(\theta)\right)}{\frac{\pi}{\lambda} b \sin(\theta)} \right)^2 \left(\frac{\sin\left(\frac{N\pi}{\lambda} s \sin(\theta)\right)}{\sin\left(\frac{\pi}{\lambda} s \sin(\theta)\right)} \right)^2 \quad (2.13)$$

One can note that when $N = 1$ the fraction on the right will equal 1, leaving the sinc function, or single slit diffraction. Similarly, when the slits' width b reaches 0, the left fraction would equal 1 (l'Hospital's rule), leaving multi beam diffraction. For multi slit diffraction, the sinc function (squared) will act as an envelope of the total plotted function. This is shown in Fig. 2.11 where the electric field (Fig. 2.11a) and the intensity (Fig. 2.11b) are both shown for $N = 8$ slits.

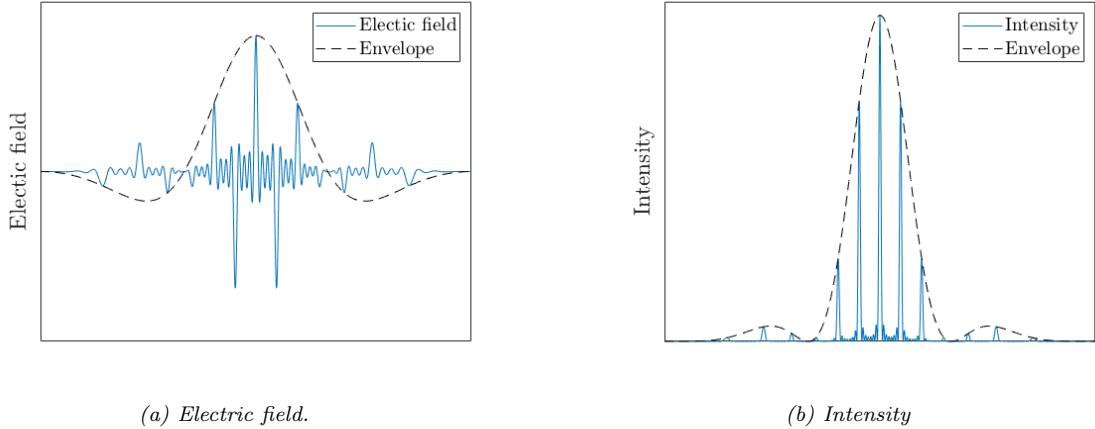


Figure 2.11: The resulting electric field (Fig. 2.11a) and intensity (Fig. 2.11b) of multi slit diffraction for $N = 8$ slits. The values are not drawn as they differ in each situation.

What one can learn from these graphs is that a diffraction pattern consists of periodic minima and maxima. These maxima are shown by high intensity peaks; the minima is the space between the maxima. So, when obtaining diffraction patterns one could analyse the pattern and recalculate the original structure of the obstruction. Or in the case with electron diffraction, the original structure

of the molecules/crystal.

In this paragraph, diffraction in just a single dimension was discussed. However, electron diffraction on rubrene will be two dimensional. Nevertheless, the multi slit diffraction can be applied on electron diffraction of rubrene, but must be considered in two dimensions.

Another difference between the discussed diffraction and the actual situation is that electromagnetic waves are scattered due to an obstacle (e.g. an aperture). When the electrons transverse the rubrene crystal, the diffraction electrons will interact with the charge of the molecules. These interaction randomly change the direction of the electrons which scatters the diffraction electrons. Due to this scattering, the electron waves can interfere and, consequently, diffract.

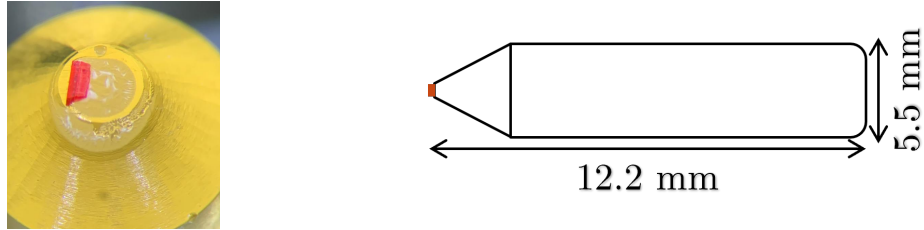
3 Methodology

This chapter will be dedicated to the description of the applied methodology of this work, encompassing the preparation method of the rubrene sample slices and conduction of the experiments. The preparation of the rubrene slices for both absorption spectroscopy and electron diffraction will be similar and is of importance for the interpretation of the results. For these reasons, the sample preparation will be explained in detail. Next, the methodologies of the actual experiments shall be discussed.

3.1 Sample Preparation

In order to cut the crystal to the desired thickness, an ultramicrotome (Leica UM C7) will be used. Microtomes are able to rotate an arm on which the crystal is attached with an additional translation to cut a slice with a diamond knife (Diatome Ultra 45°). The entire process will be explained in this paragraph.

First, the crystal is carefully glued on the tip of an epoxy resin such that the crystal is on top and cuttable with the diamond knife. In Fig. 3.1 a photo and an illustration of a rubrene crystal on the epoxy resin are displayed.

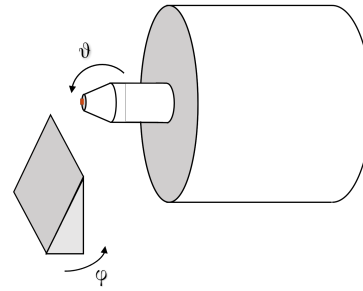
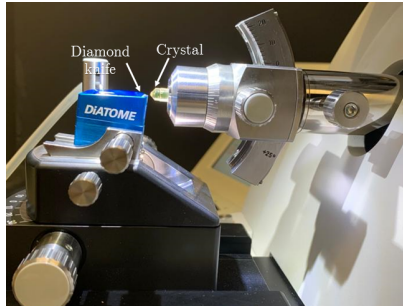


(a) An actual image of crystallised rubrene on an epoxy resin. The reddish rectangle is the rubrene crystal. (b) An illustration of the same situation as Fig. 3.1a with corresponding measures.

Figure 3.1: Fig. 3.1a is a real image of a rubrene crystal on the tip of the yellow epoxy resin. Fig. 3.1b shows an illustration of the same situation with the corresponding measures.

In the microtome, the knife shown in Fig. 3.2a does not move, instead, the crystal moves. To cut good slices, the crystal surface and the knife must be well aligned as shown in Fig. 3.2b. Recall the crystal lattices from Subpar. 2.1.3. The crystal is grown such that the crystal contains rectangular shapes. Although the rubrene crystal consists out of rectangular shapes, gluing the crystal on the resin cannot be done perfectly. There will always be an off angle. The angle of the knife and the crystal surface facing the knife must therefore be adjusted carefully to be parallel to each other. However, the crystal surface may not be parallel to the weakly-bound layers of rubrene molecules forming the crystal. Important to consider are two angles: the azimuth φ and the polar angle ϑ . The azimuth is the angle the knife makes with respect to the crystal on the horizontal plane. Rotational direction on the vertical plane is the polar angle, which is the vertical angle between knife and crystal. It is of utmost importance to reduce both in order to cut proper rubrene slices. The azimuth angle is adjusted by rotating the knife. Oppositely, the polar angle is adjusted by rotating the crystal. A photo and its simplified schematic representation of the microtome and their rotation angles is given in Fig. 3.2.

Besides aligning the knife and crystal surface, the latter must be orientated such that the longest edge is at the bottom and hits the diamond knife first. By doing this, the chance of destroying the fragile crystal is reduced, resulting in higher quality rubrene slices. In the example of Fig. 3.1a, the crystal has to be rotated approximately an additional 90°.



(a) A real image of the microtome with sample and diamond knife. (b) A schematic simplification of the microtome with sample and knife.

Figure 3.2: A photo and a sketch of the microtome with the knife and crystal.

The used ultramicrotome is capable to cut sample slices between 1 nm – 15 μm [10]. However, the knife is capable to cut 30 – 300 nm [11]. So, the diamond knife determines the restrictions of slice thickness. When the crystal nears the knife, the arm slows its rotational speed to a predefined one and moves vertically down, instead of a rotational movement, and thereby cutting a slice off the crystal. Once the slice is cut, it will float on a (distilled) water filled tub. An image of the view from the microtome's objective is displayed in Fig. 3.3.

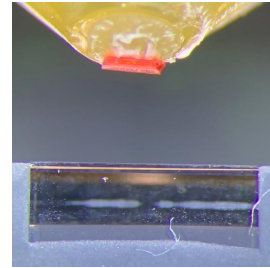


Figure 3.3: On the top, one can see the rubrene crystal (orange). Bottom of the image is the diamond knife on which the lens system is focused.

At the stage represented by Fig. 3.2a, the arm will slow down and cut the crystal. When cut, The rubrene slices will float on the distilled water. The slices can then, carefully, be picked up by a loop, which uses the water's surface tension to transport the slices, and place them on a TEM mesh grid ($\varnothing 3$ mm). TEM grids are tiny copper sheets with holes available in various shapes and hole sizes. The grid is specified in 'holes per inch', so a mesh grid of 600 would indicate that there would be 600 holes per inch. As the diameter is merely 3 millimetres, meaning that there are approximately 71 holes over the length of the diameter. Often used hole shapes are square and hexagonal shapes. Their original purpose is to hold a sample in order to examine in a Transmission Electron Microscope (TEM), the electron diffraction experiment. They can, however, also hold a sample for the absorption spectroscopy experiment. Images of the transport loop and an example of a TEM mesh grid is displayed in Fig. 3.4.

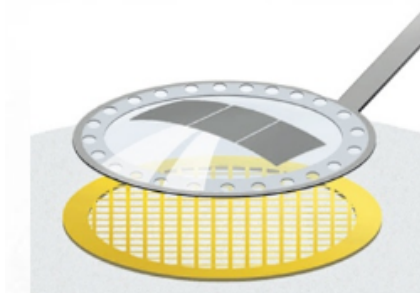


Figure 3.4: Schematic representation of a transportation loop that nears a TEM mesh grid. [12]

Note that the loop has circular holes on its edge. These holes make the drainage of the water from the loop more evenly. When the water is drained, the rubrene slices will ideally be on the TEM

mesh grid, ready for the experiments.

3.2 Absorption Spectroscopy

The goal of absorption spectroscopy is to measure a spectrum of the absorbed light of a crystal. An absorption spectrum can be measured in a solution and from a solid state crystal. By measuring absorption spectra, the efficient excitation wavelengths of rubrene can be mapped. The practice of absorption spectroscopy is shortly theoretically explained in Par. 2.2, this paragraph will elaborate on it and depend on the practical set-up and measurements.

3.2.1 Absorption Set-Up for Solid Crystallised Rubrene

To observe all absorption peaks of a sample at once, a broadband light source is used. This light can be focused on a sample slice which either reflects (or scatters), transmits, or absorbs the light. The light that is transmitted is used to calculate the absorbance. To obtain the transmission spectrum, the emission spectrum of the light source must be known before focusing it on the rubrene slice. This spectrum represents $I_0(\lambda)$ as function of the wavelength. Then, the light source can be focused on the slices. Again, the intensity $I(\lambda)$ is measured as a function of the wavelength. By measuring these intensities, the transmittance for each wavelength can be calculated with Eq. 2.5. Next, the absorbance can be calculated using Eq. 2.6.

Accurately measuring the rubrene sample slice's absorption spectrum can be achieved by focusing the light on the sample slice. Much of the light will be transmitted and absorbed this way, thereby creating a more accurate measurement. To focus the light well on the sample slice an optical set-up is used which is illustrated in Fig. 3.5.

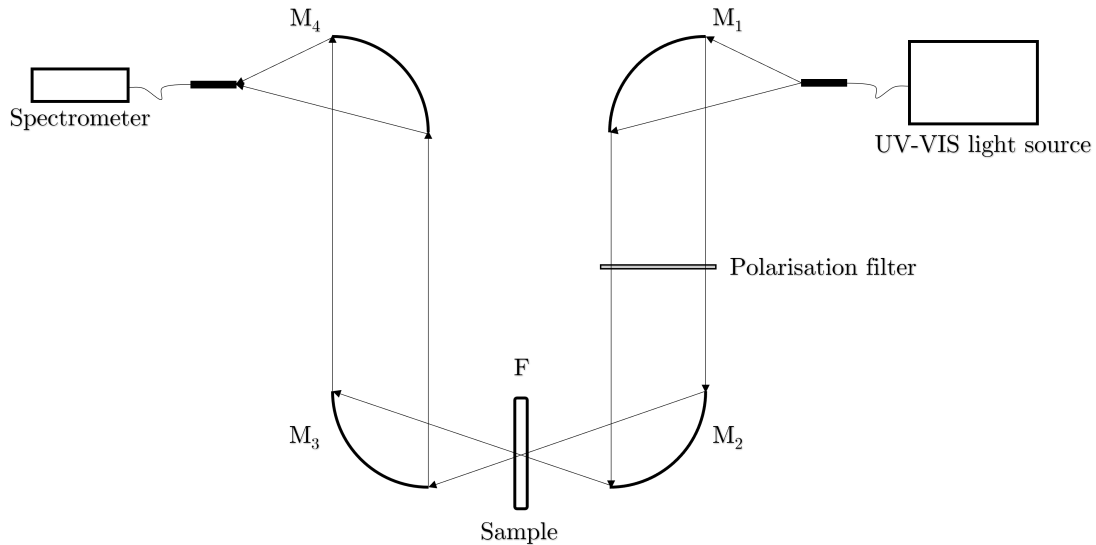


Figure 3.5: The set-up of the absorption spectrometry for a crystallised sample slice. The set-up contains four parabolic concave mirrors which either collimate or focus the light. The light of the source is approximately a point source and contains UV- and/or Vis-light. The light is then focused on the sample slice. The remaining light, after absorption, transmission and scattering, will be directed to the spectrometer. Both the light source and the spectrometer are connected with optic fibre cables.

As can be seen in the set-up's illustration, the path of the light begins with the UV-Vis light source. The UV- and Vis-light is separately generated with, respectively, a deuterium and a halogen source which can be controlled independently. Their observed spectra by the spectrometer after the optical set-up is shown in Fig. 3.6.

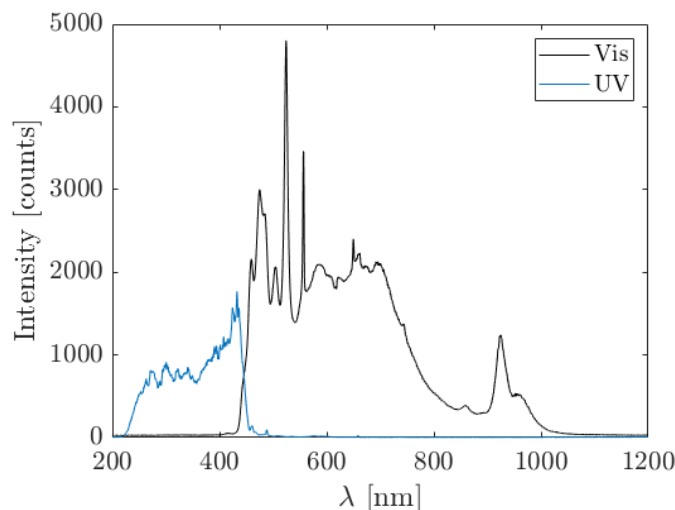


Figure 3.6: Two spectra of the used light source. The black spectrum represents the visible halogen light source whereas the blue spectrum represent the ultra violet deuterium light source.

The light is transported via an optic fibre cable. The exiting light is approximately a point source. Next, the light is reflected by the first of four parabolic concave mirrors. The function of the first mirror is to reflect the light 90° and collimate it. The function of mirror M_2 is to reflect the light again 90° and focus it on the sample. There is also an option to add a polarising filter (LPVISE100-A) between M_1 and M_2 to polarise the light. On the downside, the light's intensity will significantly decrease due to a polarisation filter. The rubrene slice on the TEM grid will be placed on the focal plane by observing camera images and roughly measuring the spot size on several positions. After the rubrene slice, the light diverges again. The function of M_3 is to reflect the light towards M_4 and collimate it. Lastly, M_4 reflects the light towards the optic fibre cable of the spectrometer and focuses it.

The measurements are performed using a commercial spectrometer – Avantes StarLine AvaSpec-2048 [13] – with a resolution of 0.5 nm and commercial light source – Ocean Insight DH-2000-BAL Light Source [14] – whereas the optical set-up from Fig. 3.5 (from M_1 to M_4) is non-commercial. The focused white light has a spot size of approximately 150 μm . Practically, several spectra are obtained during the measurements, using a software written by Max Planck Institute employees. These spectra are the ambient light (which is subtracted from all other measured spectra), reference of the source (I_0), and the absorption spectrum. All are exported to text files and processed using MATLAB.

3.2.2 Absorption Set-Up for Dissolved Rubrene

Fundamentally, the set-up for the absorption spectroscopy of solid rubrene is the same as the set-up for the solvent based absorption measurement. It still uses the same physics, Par. 2.2. The largest difference between the set-ups is the state of rubrene. In the former, rubrene is crystallised and solid, in the latter, rubrene is dissolved in chloroform, CHCl_3 . Chloroform is a dipole due to the heavier chloride atoms bound to carbon. A dipole makes for a great solvent for aromatic molecules such as rubrene. Chloroform absorbs IR wavelengths, so the solvent interferes minimally with the absorption of rubrene as its expected absorption is in the range of UV-Vis [15, 16].

In this case, the sample is not cut from a crystal, but chemically prepared. For this purpose, the precious crystal is not used, but rather a rubrene powder with a purity > 98%. This was dissolved in chloroform for a concentration of $c = 0.1, 0.05, 0.01$ mmol/L [17], and poured into a cuvette, a transparent vial of 10 mm to hold the liquid.

The procedure to measure the absorption spectrum of the rubrene solution is similar to the pro-

cedure of crystallised rubrene, but is completely automatised. Only the placement of the cuvettes must be done manually. First, a blank measurement must be done in order to have a reference I_0 to calculate the absorbance. The blank measurement consist of a cuvette with pure chloroform. Although chloroform absorbs in IR, its absorption must still be taken into account. Next, the absorption of rubrene solutions can be measured. Illustrations of the measurements are shown in Fig. 3.7. These absorption measurements are done with a ThermoFisher Scientific NanoDrop 2000c Spectrophotometer¹ with a spectral range from 190 – 840 nm and a resolution of 1 nm. The data is again processed with MATLAB.

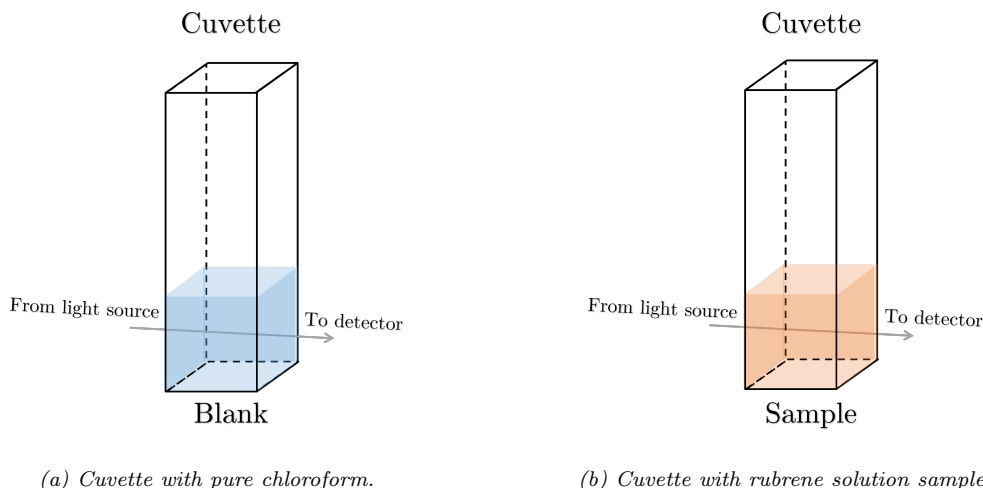


Figure 3.7: Fig. 3.7a shows the blank measurement, the cuvette with pure chloroform (actually transparent). Fig. 3.7b shows the rubrene solution with the $c = 0.1, 0.05, 0.01$ mmol/L.

3.3 Electron Diffraction

With electron diffraction, the structure of the crystal can be investigated. The obtained result will be diffraction patterns. From the patterns, one could, in principle, recalculate the crystal's structure and determine if the rubrene slice is unharmed by the preparation method, which is important information for future experiments with the specific sample slices. This experiment is conducted with a non-commercial electron diffractometer designed and built by a MPSD research group. The device is similar to a TEM in diffraction mode, but is of simpler design. A schematic is presented in Fig. 3.8.

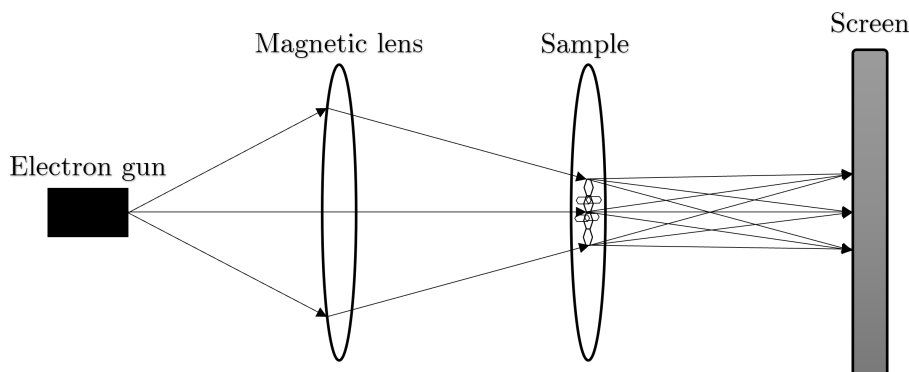


Figure 3.8: A schematic of the used diffractometer for the electron diffraction experiment.

Free electrons are produced by focusing a pulsing UV laser beam of 1000 Hz on a gold cathode in the electron gun. The electrons will travel through a (ultra) high vacuum. Vacuum is necessary to

¹Courtesy of DESY Bio-chem lab.

avoid lightning generation or ionisation of air in the device's chamber. Both would be dangerous and inefficient for the experiment. The electrons are accelerated by applying an electric field by connecting a high voltage.

Once accelerated by the electric field, the electron beam's path is focused by an applied magnetic field of the magnetic lens, which can be seen left from the sample in Fig. 3.8. The magnetic lens is, in principle, an inductive coil through which a current flows. The magnitude of the current determines the magnetic field and thus the focus of the electron beam. The smallest focal point of the beam has a size of approximately 300 μm and is highly dependent on the charge of the electron beam. The more electrons the electron pulse contains, the more the beam is repelled outwards.

As extensively discussed in Par. 2.3, will the crystallised rubrene diffract the electron beam once transmitted. The diffracted electrons will strike a phosphorescent screen which converts the electrons' kinetic energy to visible light. The light can be captured by a CCD (Charge-Coupled Device), thereby obtaining the diffraction pattern. Not all electrons are diffracted though. Because of this, a beam dump is installed between the rubrene sample and screen. The beam dump blocks the zeroth order diffraction spot which would otherwise be overly bright.

The experiment will be conducted with approximately $2 \cdot 10^3$ e^- per laser pulse. As the laser pulses with a frequency of 1000 Hz, that means $2 \cdot 10^6$ e^-/s . The CCD is able take an image with an exposure time of 30 s. To obtain a better signal ten images are taken with identical exposure time and summed. This means that the effective exposure time will be 300 s. Resulting in a total electron count of the diffraction pattern of $N_{\text{e}^-} = 6 \cdot 10^8$ e^- .

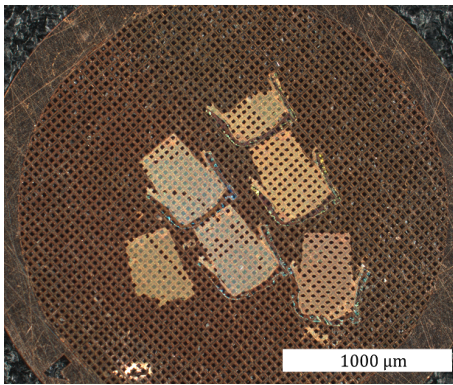
4 Results

In this chapter, several images of prepared crystal samples for the absorption and diffraction experiment will be displayed. Then, the obtained results of the conducted experiments will be presented and clarified with reference to the theory and methodology.

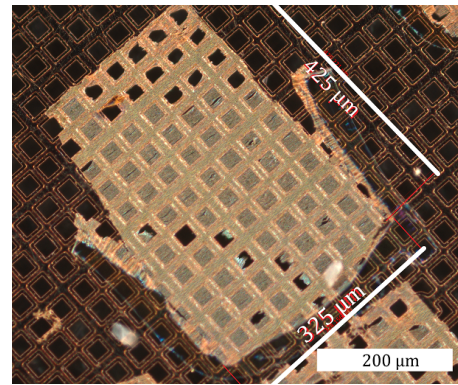
4.1 Prepared Samples

As described in Par. 3.1 the rubrene samples were required to be placed on TEM mesh grids. This paragraph will show images of the samples for the absorption spectroscopy experiment and electron diffraction experiment.

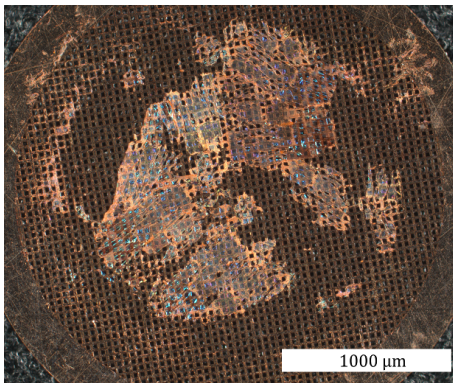
Samples slices for absorption spectroscopy were cut from two different rubrene crystals coded A3 and B3 which are believed to represent different crystal orientations in the cutting plane. The samples of the absorption experiment were placed on a TEM 600 rectangular mesh grid, and were cut on three thicknesses: $t = 250, 200, 150$ nm. When the samples were placed successfully on the grid, microscope images were made. The images of the $t = 250$ nm of the two probes are shown in Fig. 4.1.



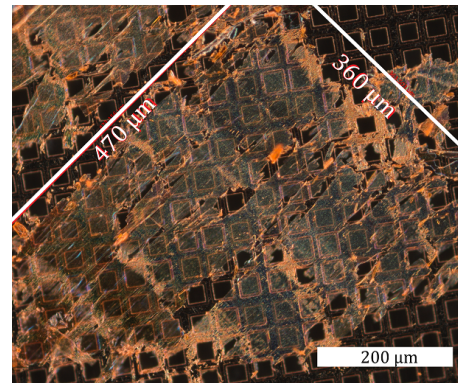
(a) Crystal A3 cut at $t = 250$ nm and placed on a 600 rectangular mesh grid. Image taken with 5 times magnification.



(b) Crystal A3 cut at $t = 250$ nm and placed on a 600 rectangular mesh grid. Image taken with 20 times magnification.



(c) Crystal B3 cut at $t = 250$ nm and placed on a 600 rectangular mesh grid. Image taken with 5 times magnification.



(d) Crystal B3 cut at $t = 250$ nm and placed on a 600 rectangular mesh grid. Image taken with 20 times magnification.

Figure 4.1: Rubrene sample cut at the thickness of $t = 250$ nm. Fig. 4.1a and Fig. 4.1b depict the crystal probe A3. Fig. 4.1c and Fig. 4.1d depict the crystal probe B3. These pictures were taken with a ‘dark field imaging’ filter making the contrast of the image more pronounced.

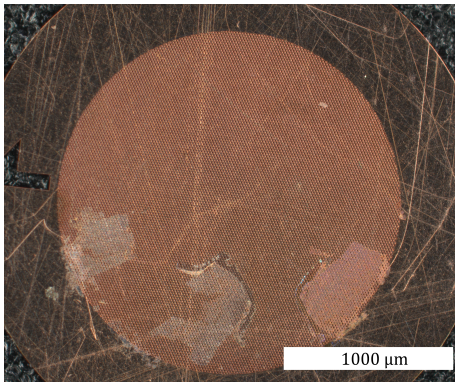
In Fig. 4.1 one can observe the prepared samples. Fig. 4.1b and Fig. 4.1d show a single sample slice, a single slice of the respective crystal. Some of the grid holes are covered by samples while others are not. This can be seen by the colour of the hole: the empty ones are black. To obtain

a useful absorption spectrum the holes of grid must be covered by crystal. In the preparation process it can happen that a slice is torn which results in uncovered grid holes as can easily be seen in Fig. 4.1b and Fig. 4.1d. When a few holes are uncovered, it will have little influence on the experiment or absorption. However, when almost all holes remain uncovered, it will become difficult to obtain a good spectrum.

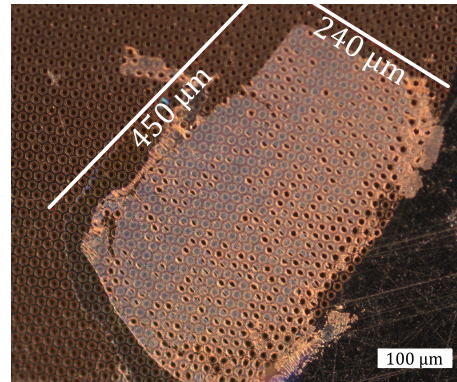
What one can immediately notice is the different shapes of the samples. Crystal A3 seems evidently more intact and forms little islands of sample. On the other hand, crystal B3 clutches more together to one big sample and has almost a fibre-like structure. This is already a great indication of different orientations cut.

As is indicated in Fig. 4.1, the samples are all roughly $450 \times 350 \mu\text{m}$. The focal point of the light was measured to be $150 \mu\text{m}$. Meaning, the samples are larger than the focal point of the white light. Thus, the white light can fully be focused on the slices.

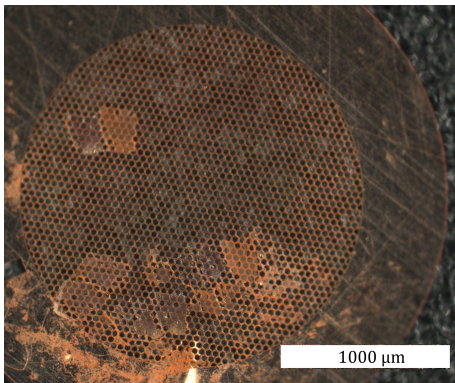
Also, it was found that thicker slices remained intact better than thinner slices. This is actually logical: the thinner the slice the more fragile it is. However, to obtain better diffraction patterns, the rubrene slices must be cut even thinner. This way, more electrons can be transmitted. For this a smaller grid can be useful (more holes per inch). The sample slices, shown in Fig. 4.2, of the electron diffraction were placed on a TEM 1500 hexagonal mesh grid. These are examples of samples for electron diffraction cut from crystal A3 and crystal B1.



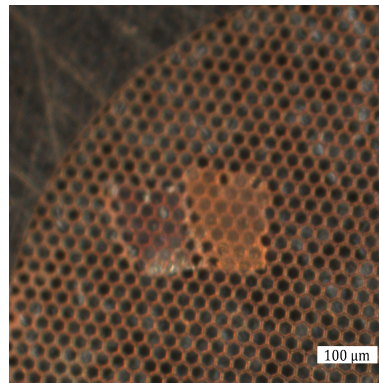
(a) Crystal A3 cut at $t = 100 \text{ nm}$ and placed on a 1500 hexagonal mesh grid. Image taken with 5 times magnification.



(b) Crystal A3 cut at $t = 100 \text{ nm}$ and placed on a 1500 hexagonal mesh grid. Image taken with 20 times magnification.



(c) Crystal B1 cut at $t = 100 \text{ nm}$ and places on a 600 Hexagonal TEM mesh grid 5 times magnification.



(d) Crystal B1 cut at $t = 100 \text{ nm}$ and places on a 600 Hexagonal TEM mesh grid 20 times magnification.

Figure 4.2: Rubrene slices cut in different thicknesses and on different TEM grids. Fig. 4.2a and Fig. 4.2b depict a slice thickness of 140 nm on a 1500 Hexagonal TEM mesh grid. Fig. 4.2c and Fig. 4.2d depict a slice thickness of 100 nm on a 600 and thus courser Hexagonal TEM mesh grid.

4.2 Absorption Spectroscopy

The absorption spectroscopy experiment is conducted with the set-ups described in Par. 3.2. The results obtained from the experiment were, of course, absorption spectra. In these spectra, the wavelength (in nanometres) is always represented on the horizontal axis. On the vertical axis, the absorbance is displayed in optical density (i.e. a logarithmic measure for the absorption, see Eq. 2.6).

4.2.1 Absorption of Dissolved Rubrene

First, the absorption for dissolved rubrene solution is presented to observe the spectral behaviour of the rubrene molecule with fewer rubrene-rubrene interactions and changes in the spectrum. With the solvent, chloroform of CHCl_3 , several concentrations rubrene solutions were made: $c = 0.1, 0.05, 0.01$ mmol/L. The measurements have been conducted for the UV-Vis range. The total UV-Vis absorption spectrum can be seen in Fig. 4.3a. Although rubrene does absorb in UV, it is not the range of interest. Fig. 4.3b zooms in on the more interesting Vis-spectrum.

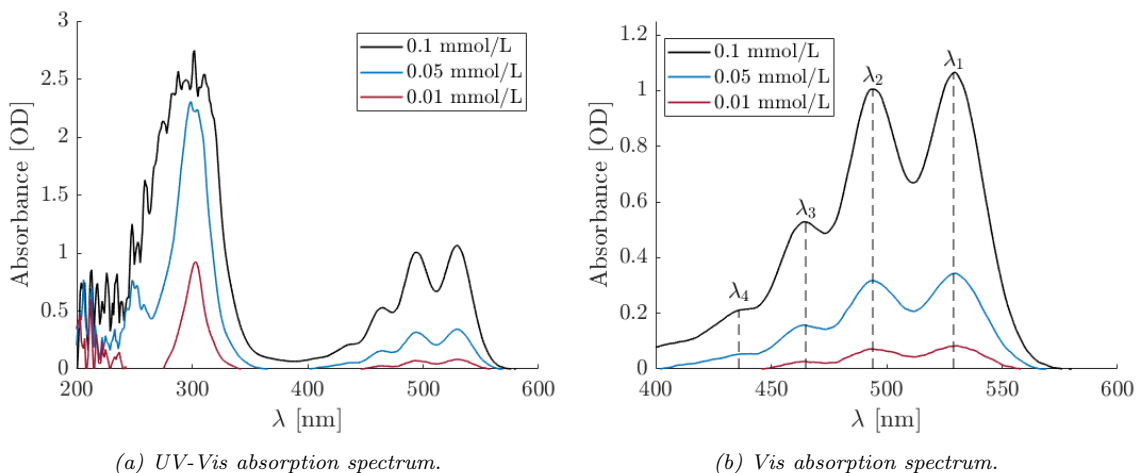


Figure 4.3: Left (Fig. 4.3a), the absorption spectrum in UV-Vis spectrum range; right (Fig. 4.3b), the absorption spectrum in Vis-range. Both contain the spectra of the concentrations $c = 0.1, 0.05, 0.01$ mmol/L dissolved in chloroform. In Fig. 4.3b, the absorption peaks, which are numbered from low to high energies, are also indicated.

In the absorption spectra, four distinctive peaks can be detected on the visible spectra. The found peak absorption wavelengths and wavenumbers, which is defined as $k = \frac{1}{\lambda}$, are listed in Tab. 4.1.

Table 4.1: Peak absorption wavelengths with corresponding wavenumbers.

Wavelength [nm]		Wavenumber [cm^{-1}]	
λ_1	529.5	k_1	18886
λ_2	494	k_2	20243
λ_3	465	k_3	21505
λ_4	436	k_4	22936

From the absorption spectra, the peak wavelengths are determined for all concentrations which deviate maximally ± 1 nm, which is also the accuracy of the instrument [18]. The difference between absorption bands is on average $\Delta k = 1350 \text{ cm}^{-1}$. This agrees with values found in literature [17, 19, 20] by ± 0.5 nm or $\pm 7 \text{ cm}^{-1}$.

As discussed in the theory, Subpar. 2.2.1, an equidistant peak wavenumber structure is an indication for vibronic progression. Meaning, when a molecule is excited into another electronic orbital, there is a chance the molecule will also be excited into another vibronic energy level due to

the Frank-Condon principle. Like always in quantum mechanics, this is not a definite occurrence, but a probability. The molecule can only be excited by the correct energy, but not all incident photons with the correct energy are absorbed. Thereby creating a chance to also excite the molecule to a higher vibronic state, which explains the equidistant structure of the absorption spectra.

At the peak wavelengths of the rubrene concentration of $c = 0.1$ mmol/L, the absorption coefficients ε are determined using Eq. 2.6 and are presented in Tab. 4.2.

Table 4.2: Absorption coefficients at the peak wavelength for the rubrene concentration $c = 0.1$ mmol/L.

λ [nm]	ε [$\cdot 10^3 \text{ M}^{-1} \text{ cm}^{-1}$]
529.5	10.7
494	10.0
465	5.28
436	2.11

In Fig. 4.3, one can see that for the concentration $c = 0.1$ mmol/L the UV range is rather spiky. This is due to a too high saturation of the solution. This effect is still present at the concentration of $c = 0.05$ mmol/L, but is clearly lessened. At a concentration of $c = 0.01$ mmol/L the effect is not present for the UV- or Vis-spectrum. For more diluted solutions the effect lessens. In the Vis-range, on the other hand, no such effect can be detected. As the range of interest is the visible spectrum, this measurement is still valid.

4.2.2 Absorption of Crystallised Rubrene

In this section, the obtained results from the absorption spectroscopy of crystallised rubrene is presented. Because absorption is polarisation dependent in anisotropic media, such as crystallised rubrene, both non-polarised and polarised absorption spectra are shown. First, the absorption spectra of probes with a sample thickness of $t = 250, 200, 150$ nm of two crystals, represented by Fig. 4.4.

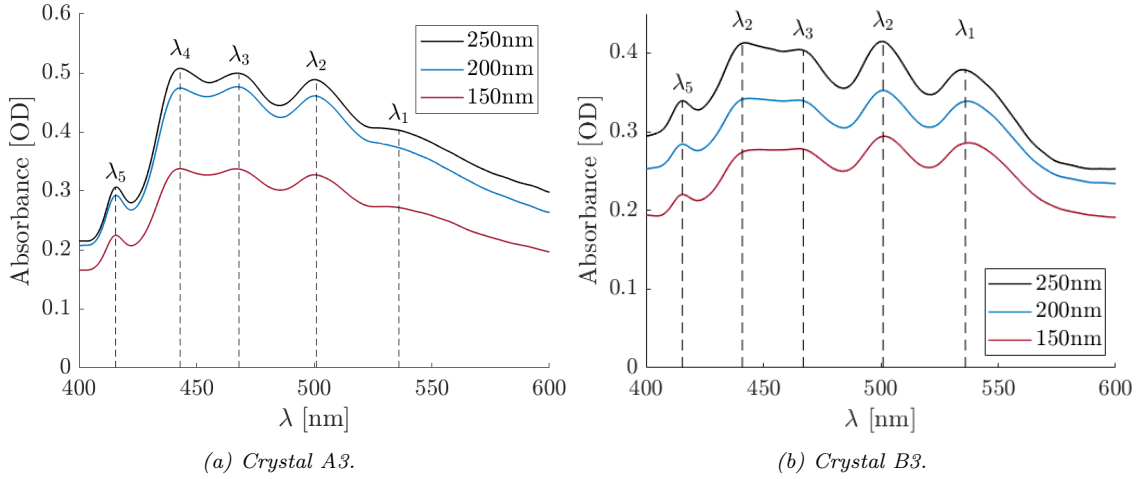


Figure 4.4: The absorption spectra of two crystals at thickness $t = 250, 200, 150$ nm. These measurements are conducted with unpolarised light. A Gaussian data smoother is used to present the spectra.

Five distinctive peak wavelengths were found for both crystals with a deviation of ± 0.5 nm or $\pm 20 \text{ cm}^{-1}$ and summarised in Tab. 4.3.

Table 4.3: The wavelengths and wavenumbers of the absorption spectra shown in Fig. 4.4. The absorption peaks are listed from low to high energies.

Wavelength [nm]		Wavenumber [cm ⁻¹]	
λ_1	536	k_1	18657
λ_2	501	k_2	19960
λ_3	467	k_3	21413
λ_4	441	k_4	22676
λ_5	415.5	k_5	24067

From these numbers, a vibronic progression is determined of an average $\Delta k = 1353 \text{ cm}^{-1}$ which approximates values found in literature [19] by $\pm 0.6 \text{ nm}$ or $\pm 21 \text{ cm}^{-1}$.

What one can notice from the Fig. 4.4a and Fig. 4.4b is the different shape of the spectra. In Fig. 4.4a the first peak λ_1 is just barely visible, whilst it is highly pronounced in Fig. 4.4b. Nevertheless, the values of the peak wavelengths of the two crystals seem to match well.

Also note that an extra absorption band is present in the absorption spectra of the both rubrene crystals, Fig. 4.4, compared to the solvent based experiment, Fig. 4.3. This is the lowest wavelength and thus the highest energy transition. Also, the peak absorption wavelengths of the crystallised rubrene are redshifted compared to the dissolved rubrene, due to the interactions with its neighbouring molecule. The crystal shift is mentioned in Subpar. 2.2.2. A molecular crystal will absorb slightly larger wavelengths, lower energy photons, than its uncrystallised counterpart. The average measured redshift is $\Delta\lambda_r = 5 \text{ nm}$ which corresponds to a wavenumber and energy difference of $\Delta k_r = 222 \text{ cm}^{-1}$ and $\Delta E_r = 27 \text{ meV}$, respectively.

When polarising the white light with a polarisation filter, one can rotate the filter and thereby select a polarisation. This is done for 0° until 180° with steps of 45° , because of the symmetrical characteristics of linear polarised light. The absorption spectra of the polarisation angles can be seen in Fig. 4.5. The used sample was cut from crystal A3 at a thickness of 120 nm and placed on a TEM mesh 1500 hexagonal grid. The polarising filter not only polarises the light, but also filters UV-light [21]. Due to this, just the Vis-range is shown in Fig. 4.5.

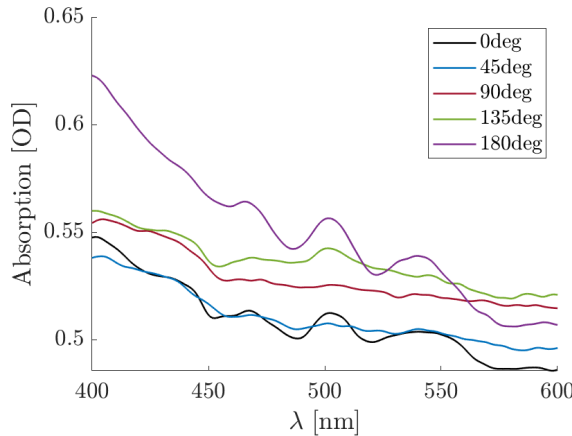


Figure 4.5: Absorption as a function of the wavelength where the polarisation of the light is rotated. Crystal A3 is used for this measurement, cut at $t = 120 \text{ nm}$, and placed on a 1500 hexagonal mesh. A Gaussian data smoother is used to present the spectra.

One can clearly see the shape of the spectra changing. At a rotational angle of 0° , there are some absorption peaks visible. When rotating the polarisation filter further, the peaks disappear. At 180° the absorption peaks appear again. As discussed in Subpar. 2.2.2, when rotating the light's polarisation (or the crystal slice), the absorption can change. This is due to the orientation of

the molecules within the crystal. When the tetracene compound's nodal plane is perpendicular to the vibrational direction of the polarised light, it will absorb. Oppositely, when the tetracene compound is parallel to the vibrational direction of the polarised light, it will not absorb. This phenomenon is clearly shown by Fig. 4.5.

4.3 Electron Diffraction

In this paragraph, several images are shown of diffraction patterns. Firstly, the simulation will be shown, analysed, and discussed for three crystal orientations from Fig. 2.7. The cut crystals for the electron diffraction were crystal A3 and B1. It is hypothesised that these were of different orientation, so one would expect different diffraction patterns from the rubrene crystal. These will then be presented, analysed, discussed, and compared to the simulated diffraction pattern.

4.3.1 Simulated Electron Diffraction Patterns

First of all, let's consider orthorhombic rubrene crystal from Fig. 2.7 made in CrystalMaker. Each edge length is given in Tab. 2.2. From theory Subpar. 2.1.3 and Par. 2.3, one can learn that a smaller edge length of the crystal's unit cell will result in a larger distance between consecutive diffraction spots, or, oppositely, a larger edge length of the crystal's unit cell will result in a smaller distance between maxima. So, it is expected that a will have the smallest distance between maxima, b will have the largest, c will be intermediate, or $d_a < d_c < d_b$.

All electron diffraction patterns are simulated using CrystalMaker and SingleCrystal. The simulated electron diffraction pattern of crystal orientation A will be presented first, Fig. 4.6. This pattern corresponds to Fig. 2.7a.

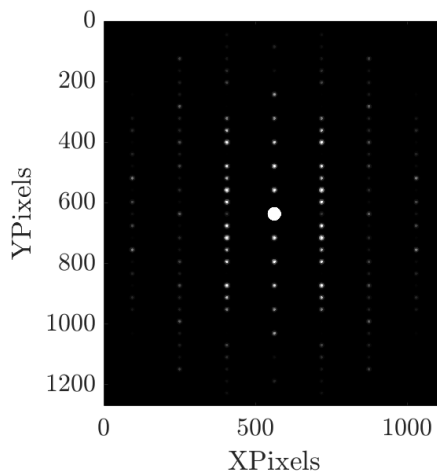
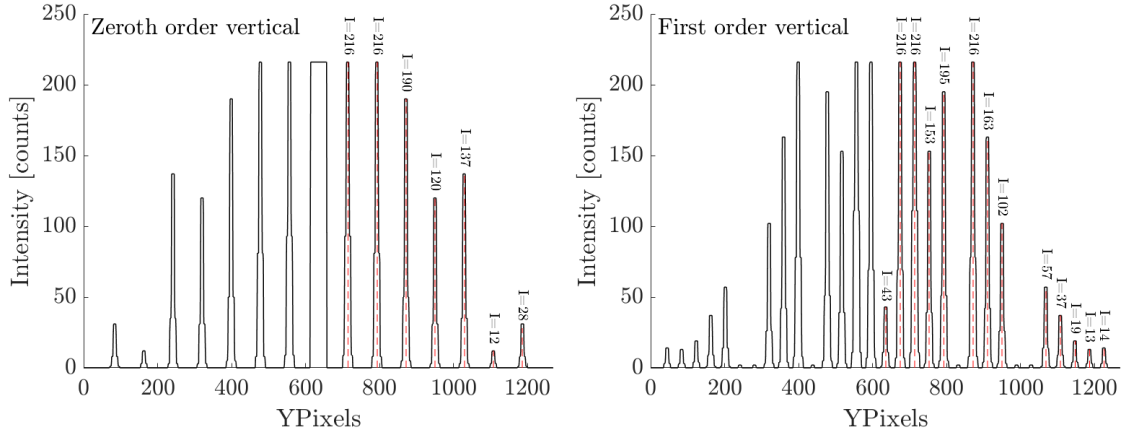


Figure 4.6: Simulated diffraction pattern of rubrene crystal on orientation A, Fig. 2.7a. The horizontal and vertical axis of the image represent the pixels, which are square in the image. Note that the used colour scale is linear. Figure extracted from CrystalMaker and SingleCrystal.

Notice that the diffraction pattern is mirror symmetric on the zeroth order vertical and horizontal line. The zeroth and first order vertical line are pronounced best. In addition, the zeroth order vertical line seems to have a smaller periodicity than the first order. Intensity of these vertical lines are plotted with respect to their position in the image, Fig. 4.7. As the first order left and right of the zeroth order vertical line are exactly the same, just one will be shown.



(a) Rubrene crystal orientation A zeroth order vertical line. In the figure, the intensity in counts is plotted with respect to the vertical pixels of the simulated diffraction pattern, Fig. 4.6. (b) Rubrene crystal orientation A first order vertical line. In the figure, the intensity in count is plotted with respect to the vertical pixels of the simulated diffraction pattern, Fig. 4.6.

Figure 4.7: The plotted intensities of the zeroth and first order vertical line of crystal orientation A.

In the graphs of Fig. 4.7, the prior observation of a different periodicity is ascertained. From these graphs, the distance between maxima of the vertical lines is determined. The distance between consecutive maxima for the zeroth and first order vertical line (V) is $\Delta y_0 = 39.3$ pixels and $\Delta y_1 = 78.8$ pixels, respectively, meaning $\Delta y_0 = 2\Delta y_1$. The horizontal order lines do not show a change in periodicity. The distance between consecutive horizontal (H) maxima is determined to be $\Delta x = 158$ pixels, which is twice the distance between maxima on the zeroth order line $\Delta x = 2\Delta y_0$. The ratios between the two is given by $H/V = 2.01$ or $V/H = 0.497$.

Next, the simulated electron diffraction pattern of crystal orientation B will be presented, Fig. 4.8. This pattern corresponds to Fig. 2.7b.

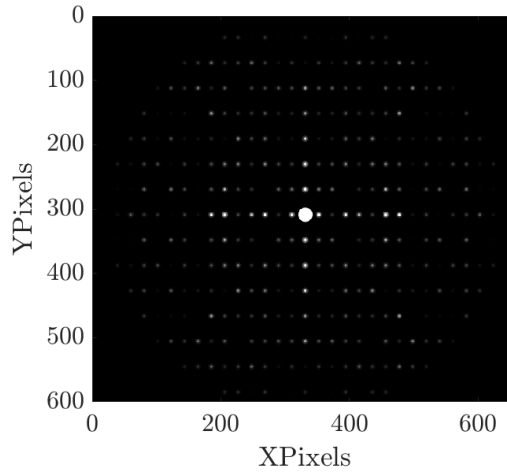
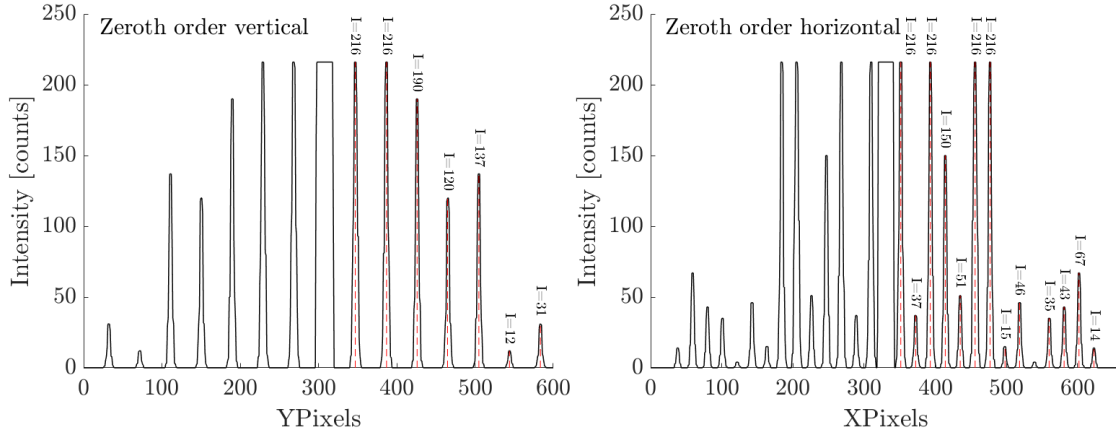


Figure 4.8: Simulated diffraction pattern of rubrene crystal on orientation B, Fig. 2.7b. The horizontal and vertical axis of the image represent the pixels, which are square in the image. Note that the used colour scale is linear. Figure extracted from CrystalMaker and SingleCrystal.

Again, the electron diffraction pattern is twice mirror symmetric. Oppositely from crystal orientation A, this pattern contains strongly pronounced zeroth order lines. Moreover, the pattern of orientation B does not contain changes in periodicity in the same direction. Intensity of the zeroth order vertical and horizontal are plotted with respect to their position in the image, Fig. 4.9.



(a) Rubrene crystal orientation B zeroth order vertical (b) Rubrene crystal orientation B zeroth order horizontal line. In the figure the intensity in counts is plotted with respect to the vertical pixels of the simulated diffraction pattern Fig. 4.8.

Figure 4.9: The zeroth order horizontal and vertical line of crystal orientation B.

In the graphs of Fig. 4.9, the intensity peaks of the zeroth order horizontal and vertical can be seen. From these graphs, the distance between consecutive maxima is determined for the horizontal and vertical direction. The distance on the zeroth vertical line is $\Delta y = 39.4$ pixels; the distance on the zeroth vertical line is $\Delta x = 20.9$ pixels. From these values, the ratios between the vertical and horizontal distances are given $H/V = 0.530$ or $V/H = 1.89$.

Lastly, the simulated electron diffraction pattern of crystal orientation C will be presented, Fig. 4.10. This pattern corresponds to Fig. 2.7c.

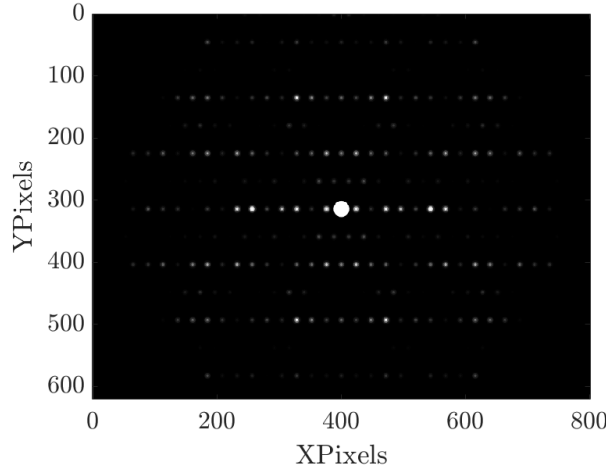
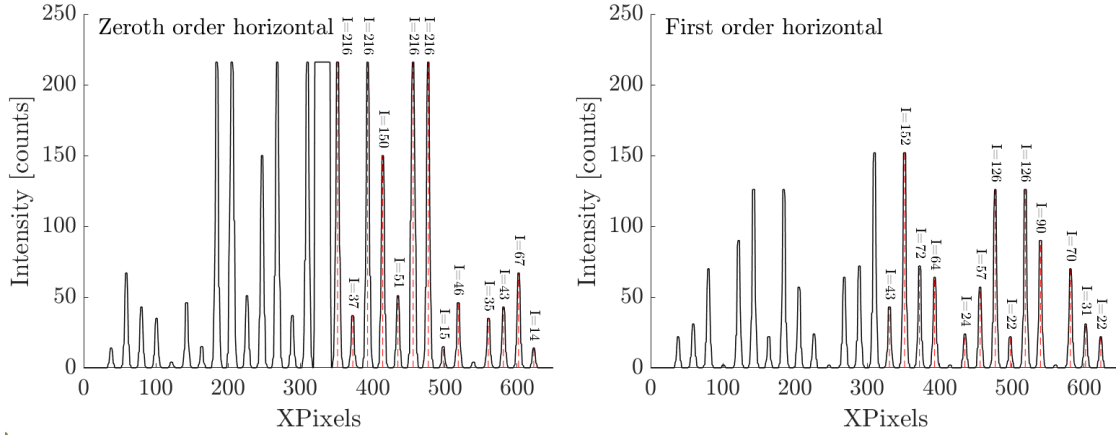


Figure 4.10: Simulated diffraction pattern of rubrene crystal on orientation C, Fig. 2.7c. The horizontal and vertical axis of the image represent the pixels, which are square in the image. Note that the used colour scale is linear. Figure extracted from CrystalMaker and SingleCrystal.

Also this electron diffraction pattern is twice mirror symmetric. This orientation's diffraction pattern seems to have strong vertical lines and a large space difference between horizontal and vertical maxima. This diffraction pattern, also, does not contain a periodicity difference in the same direction. The intensity of the zeroth order horizontal lines seems brightest of all horizontal order lines. Intensity of the zeroth and first horizontal lines are plotted with respect to their position in the image, Fig. 4.11.



(a) Rubrene crystal orientation C zeroth order horizontal line. In the figure the intensity in counts is plotted with line. In the figure the intensity in counts is plotted with respect to the vertical pixels of the simulated diffraction pattern, Fig. 4.10. (b) Rubrene crystal orientation C first order horizontal line. In the figure the intensity in counts is plotted with respect to the vertical pixels of the simulated diffraction pattern, Fig. 4.10.

Figure 4.11: The zeroth and first order horizontal line of crystal orientation C.

In the graphs of Fig. 4.11, the intensity peaks of the zeroth and first order horizontal can be seen. From these graphs the horizontal and vertical distance between consecutive maxima is determined. It is determined that the both horizontal and vertical direction do not have changes in periodicity. However, the distance between horizontal and vertical maxima are observed to be different. The distance between horizontal maxima is $\Delta x = 20.9$ pixels, whilst the distance between vertical maxima is $\Delta y = 78$. From these values the horizontal-vertical ratio is determined to be: $H/V = 0.268$ and $V/H = 3.73$.

Also from the unit cell's edge lengths, horizontal-vertical ratios can be determined. Because of the inverse effect of edge length and maxima distance, one would expect that the ratios would also be inverted. Which is confirmed and noted in Tab. 4.4. What can also be seen, is the edge length having approximately the same corresponding distance between diffraction maxima.

Table 4.4: A summary of the simulated results per orientation. The first second column shows the results from the diffraction images; the fourth column shows the results from the known edge lengths of the crystal's unit cell.

Orientation A			
Δx_A	79.0 pixels	b	7.170 Å
Δy_A	39.3 pixels	c	14.211 Å
H/V	2.01	H/V	0.505
V/H	0.497	V/H	1.98
Orientation B			
Δx_B	20.9 pixels	a	26.789 Å
Δy_B	39.4 pixels	c	14.211 Å
H/V	0.530	H/V	1.89
V/H	1.89	V/H	0.530
Orientation C			
Δx_C	20.9 pixels	a	26.789 Å
Δy_C	78.0 pixels	b	7.170 Å
H/V	0.268	H/V	3.74
V/H	3.73	V/H	0.268

4.3.2 Practically Determined Electron Diffraction Patterns

To obtain practical images of electron diffraction patterns, the electron diffractometer from Par. 3.3 was used. In the diffractometer, an electron beam is produced which is accelerated with an electric field and focused with a magnetic field. While taking electron diffraction images, the unfocused electron beam was used to search the samples, Fig. 4.12. Once located, the electron beam was focused on the examined sample. When totally unfocused, Fig. 4.12a, the sample's shadow image was rather sharp and can one clearly see the mesh grid. The more the electron beam was focused, the vaguer the image became, Fig. 4.12b and Fig. 4.12c, until the focus became too bright to recognise any samples, Fig. 4.12d. If one looks carefully, the first diffraction spots can be seen at an exposure time of just one second. The brightest zeroth order spot is blocked by the beam dump during the actual measurements.

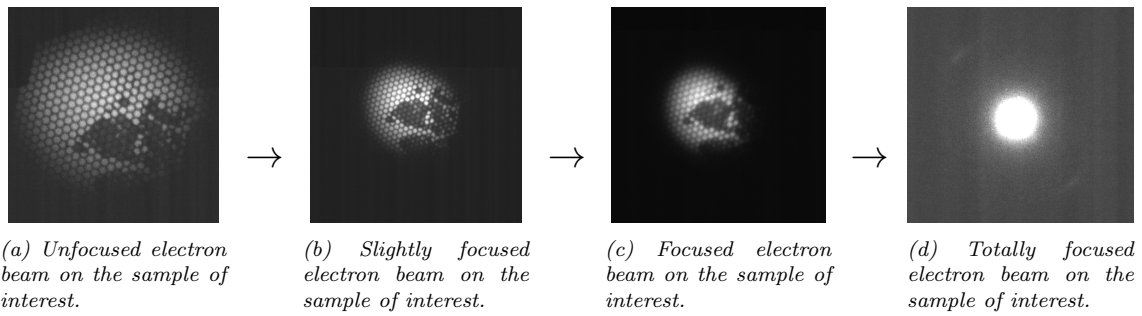


Figure 4.12: An example of the electron beam that is focused on a sample. Images taken with an exposure time of one second.

The electron diffractometer operated at an acceleration voltage of $U = 35$ kV. Diffraction patterns were determined of two crystal samples which were believed to be cut on crystal planes, coded A3 and B1. Fig. 4.13 shows the electron diffraction pattern of crystal A3 with an effective exposure time of 300 s. Note that the colour scale is logarithmic.

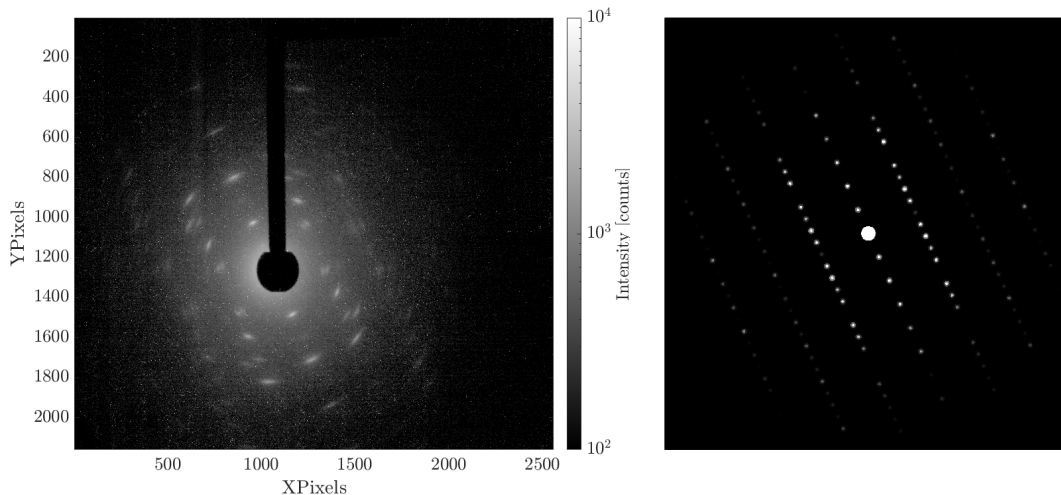


Figure 4.13: Left: electron diffraction of crystal A3 at $U = 35$ kV and an effective exposure time of 300 s. Note that both axis contain pixel counts on equal axis, and that the colour scale is logarithmic. Right: rotated simulated electron diffraction result of orientation A to support visual comparison.

What one can notice in Fig. 4.13 is the resemblance with the electron diffraction pattern of orientation A, Fig. 4.7 and also on the right side of the figure for visual comparison. The zeroth order seems to have a smaller periodicity than the first order, which corresponds with orientation A. In addition, the zeroth and first order diffraction lines have similar intensities, which is not the case at

orientation C. Furthermore, the horizontal-vertical ratios have been determined to be $H/V = 2.00$ and $V/H = 0.500$. This corresponds extremely well with simulation of orientation A.

Fig. 4.14 shows the electron diffraction pattern of crystal B1 with an effective exposure of 300 s. Note that the colour scale is logarithmic.

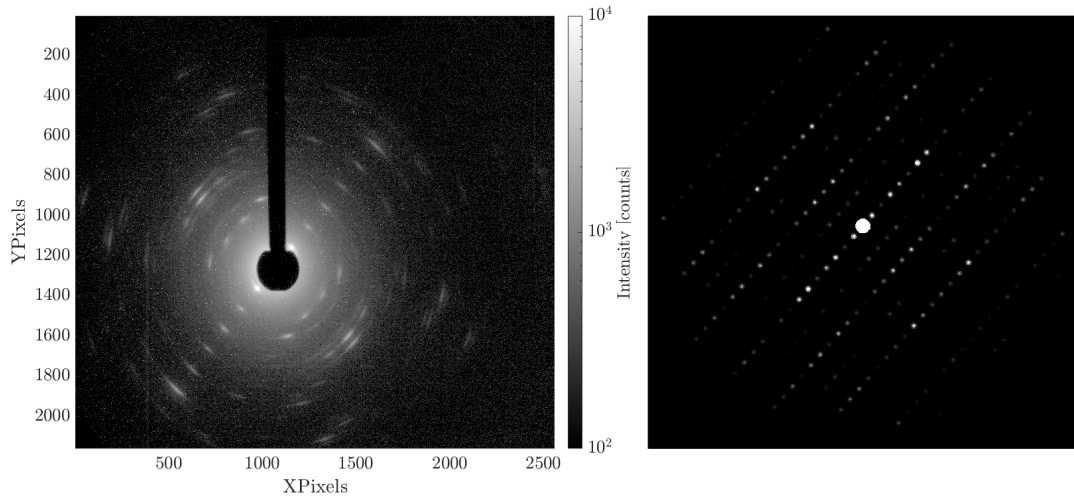


Figure 4.14: Left: electron diffraction of crystal B1 at $U = 35$ kV and an effective exposure time of 300 s. Note that both axis contain pixel counts on equal axis, and that the colour scale is logarithmic. Right: rotated simulated electron diffraction result of orientation C to support visual comparison.

What one can notice in Fig. 4.14 is the resemblance with the electron diffraction pattern of orientation C, Fig. 4.11 and also on the right side of the figure for visual comparison. The determined diffraction pattern is rather messy. This is due to the focusing the electron beam on a broken sample. The first order lies further than the pattern suggests, as the seemingly first order has maxima where one would expect a minimum. The distance between consecutive maxima, however, does not change excluding the possibility of orientation A. Moreover, the horizontal-vertical ratios have been determined to be $H/V = 0.272$ and $V/H = 3.68$. This also corresponds well with simulation of orientation C.

5 Discussion

In this chapter the methodology and results will be discussed on their accuracy and validity. This will encompass the preparation of the samples, absorption spectroscopy, and electron diffraction.

An ultramicrotome's original purpose is to thinly prepare organic tissue for examination. By applying this technique to organic crystals, nanometres thick crystal slices could be cut. With a more traditional method of preparation, this result would not be attainable. These methods etch a small part of the crystal until a fraction of it is thin enough. This is not only a wasteful methodology for these precious crystals, but also a more inefficient one compared to microtoming. Microtoming the rubrene crystal resulted in equally thin crystal samples throughout the entire sample surface. This way, measurements can be done on every part of the rubrene sample.

Rubrene molecules in its crystal bind to each other with the van der Waals bond. As it relies on the dipole moment of the molecules, which are small charges, the van der Waals bond is weak. Due to this, the rubrene crystal is very brittle which makes preparing the samples more difficult. When placing the samples on the TEM mesh, the samples tended to tear. Even the thickest samples, sometimes, had uncovered meshes. An example of this can be seen in Fig. 4.1b where the black squares are the uncovered mesh holes.

Although some mesh holes were left uncovered by the rubrene sample, absorption spectra and electron diffraction results could be obtained from these samples. For the absorption spectroscopy, the focal point was smaller than the actual sample, thereby only needing a fraction of the sample to obtain an absorption spectrum. The electron beam of the diffraction experiment, however, has a similar size as the sample. This means that, evidently, some electron will be transmitted through the TEM grid without being scattered. For this reason, the beam dump is installed.

The absorption spectra are measured for dissolved rubrene and crystallised rubrene. Their methodologies are explained in Par. 3.2. The set-up of the solvent based absorption spectroscopy was fully automated by the commercial device. Meaning, the accuracy of the measurement and results are given by the manufacturer. The accuracy of the absorption spectroscopy in UV-Vis was ± 1 nm. This deviation was also found when analysing the peak absorption wavelengths. Inaccuracies were found in the UV-range of the measured spectra. But, as UV-spectrum was not the region of interest, the measurements were still valid.

The absorption set-up for the crystallised rubrene was partially commercial and partially non-commercial. The optical set up was used to focus the light on the sample. This set-up, however, contained some flaws. Due to the concave mirrors, astigmatism was introduced in the white light beam. This made the beam elliptical. Nevertheless, the focal point size remained smaller than the sample size. Also, when adding and rotating the polarisation filter, the focal point of the white light also rotated. Due to this, every time when selecting another polarisation, the position of the optic fibre of the spectrometer had to be optimised. These realignments introduce an inaccuracy in the experiment. This also explains why the 0° and 180° absorption spectrum in Fig. 4.5 have a similar shape but different optical density when theoretically they should be identical. During the analysis of the polarised absorption, merely the shape of the spectra is considered, thereby eliminating this specific problem. Besides, the polarisation filter filtered not only polarisation, but also the entire UV spectral range. Possible information could not be obtained because of the filtering. On top of that comes the accuracy of the Avantes spectrometer which is ± 0.5 nm. A deviation which was also observed in the results.

Both absorption of dissolved rubrene and crystallised rubrene show phenomena described in theory Par. 2.2, such as the vibronic progression of the absorption spectrum and red shift of the crystallised rubrene absorption peaks. Besides, the vibronic progression found in the absorption spectra of both solvent based and crystallised rubrene agree with literature with just small deviation: ± 0.5 nm or ± 7 cm^{-1} for solvent based, and ± 0.6 nm or ± 21 cm^{-1} for the crystallised absorption spectrum. In addition, the average values of the determined vibronic progression differ

merely 3 cm^{-1} .

The simulated electron diffraction pattern for orientation A, B, and C were all linked to theory and the unit cell's edge lengths, which were known parameters. Moreover, could the distance between horizontal and vertical consecutive maxima be referred back to the unit cell's edge lengths. All pixel counts and location of simulated maxima and order lines were determined with MATLAB, but had a small deviation up to ± 1 pixel.

One of the first times the home-built diffractometer was used, was to determine the diffraction patterns of rubrene. Before this, the electron beam was optimised, characterised, and tested on a well scattering sample (high atomic number Z) which resulted in a clear electron diffraction pattern. By using a Faraday cup, the charge of the electron beam could be measured indirectly. This device is connected to an electrometer, which can detect extremely small currents. From these, values an electron count could be estimated: $N_{e^-} = 6 \cdot 10^8 \text{ e}^-$ per measurement which lasts $10 \cdot 30 \text{ s}$.

To obtain a diffraction pattern a longer exposure time is necessary than (a fraction of) a second. The camera was able take an image with an exposure of maximally 30 s . This exposure time, however, did not quite satisfy. A diffraction pattern of crystallised rubrene can be seen after 30 s , but it is still vague. To solve this particular problem multiple images were taken, cumulatively. As an exposure time of 300 s was desired, ten images were taken. After a background image was taken and subtracted from all ten, every individual image was summed to obtain an electron diffraction pattern image with an exposure time of 300 s .

Prior to the measurement, it was hypothesised that crystal A3 and B1 were cut on crystal planes. Due to this suspicion, the presented electron diffraction patterns, Fig. 4.13 and Fig. 4.14, have been linked to suspected crystal orientations. The diffraction pattern were, firstly, studied and compared visually. Although one can see the comparison between measured and simulated results, not merely the presented images were used for analysis. Also, other diffraction patterns of the same crystal were used in the analysis. After, the horizontal-vertical ratios were determined which corresponded very well to simulated results, ± 0.06 maximally.

When considering the molecular rubrene unit of the crystal in orientation A, Fig. 5.1, one can notice the tetracene compound's nodal plane is orientated diagonally. Light will in this case be directed perpendicular onto the crystal plane of orientation A. Photons are only absorbed by the tetracene compound when it vibrates perpendicular to the nodal plane. This is actually the true if one rotates the crystal or the polarisation of the light. A phenomenon that is observed in Fig. 4.5 for the same crystal A3. If this is practically true for other crystal orientations, too, is not known. The polarised absorption spectra and electron diffraction pattern of crystal A3 of crystal orientation A3 are not contradictory.

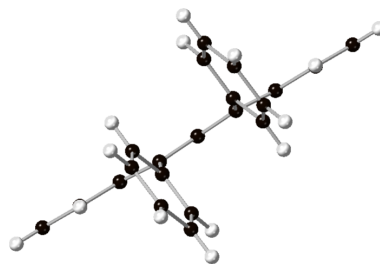


Figure 5.1: Molecular unit in crystal orientation A.

6 Conclusion

The goal of this project was to optically and structurally characterise the ground state of an organic molecular rubrene crystal. The spectroscopic characterisation of the rubrene crystal is done by absorption spectroscopy. Absorption spectra of the molecule in solution and molecular crystal could give useful information of excitation wavelengths of the molecule and their vibronic energy states. The structural characterisation of the crystal is conducted by an electron diffraction experiment. Electron diffraction patterns would be able to map the orientations of the cut crystals and their structure. However, for both experiments the penetration depth of light and electron was too small for thick samples. To solve this problem, the crystal samples were prepared with an ultramicrotome in the order of $t = 100$ nm

The ultramicrotome prepared samples for both absorption spectroscopy and electron diffraction experiment were placed on TEM mesh grids. The samples of absorption spectroscopy could be afforded to be thicker than the samples of electron diffraction. Eventually, the samples for the absorption were cut at three thicknesses: $t = 250, 200, 150$ nm, while the sample for the electron diffraction were cut at the thickness of $t \leq 100$ nm.

Absorption spectroscopy is conducted in two different molecular states: dissolved and crystallised rubrene. Dissolved rubrene shows slightly different spectroscopic behaviour than crystallised rubrene. For instance, the crystallised rubrene shows different shapes absorption spectra than dissolved rubrene, but, in all absorption spectra, equidistant peak wavelengths are observed. The peak absorption wavelengths of rubrene crystal are observed to be redshifted with an average of $\Delta\lambda_r = 5$ nm, $\Delta k_r = 222$ cm⁻¹, or $\Delta E_r = 27$ meV. Meaning, that the binding energy of the π -electrons of crystallised rubrene molecules is slightly lower than its molecular counterpart. A phenomenon predicted by theory and practically substantiated. However, both experiments show practically identical vibronic progression in their absorption spectra of $\Delta k = 1350$ cm⁻¹. The absorption wavelengths of crystallised rubrene have conclusively shown to be $\lambda = 536, 501, 467, 441, 415.5$ nm, in the order of low to high energy, for several samples. Indicating that $\lambda = 536$ nm would be the most efficient wavelength to excite the crystal without too much energy loss. Furthermore, there is not enough data obtained to give a conclusive answer on the absorption behaviour of rubrene crystal in the three orientations indicated by Fig. 2.7. However, the polarisation absorption measurements have shown that crystallised rubrene is indeed polarisation dependent.

In the three specified crystal orientation from rubrene's unit cell, Fig. 2.7, the electron diffraction pattern is simulated. These simulated diffraction pattern were analysed visually and objectively with the ratios between distances. Visually, orientation A, B, and C are different from each other. Orientation A contains a clear shift in periodicity in a zeroth order line; Orientation B had an equally bright zeroth horizontal and vertical which was not the case with the other orientations; Orientation C resembled orientation A, but did not have a change in periodicity in any of its diffraction lines. For the more practical part, electron diffraction is conducted in the home-built electron diffractometer.

The crystals used in the experiment were believed to be cut on a crystal plane. However, which crystal plane one was regarding was unknown. In Par. 4.3, only one diffraction pattern per crystal is presented, however more diffraction pattern images were taken and included in the visual comparison and analysis. On a visual aspect, crystal A3 could be argued to resemble orientation A's simulation. Objectively, the ratios of crystal A3 were determined to be $H/V = 2.00$ and $V/H = 0.500$. In addition, the polarised absorption spectra of crystal A3 do not contradict the these observation of the electron diffraction pattern. Thereby, crystal A3 is conclusively identified as crystal orientation A with the unit cell's edge length b and c . Visually, one can see a resemblance between crystal B1 and orientation C. The ratios were determined to be $H/V = 0.272$ and $V/H = 3.68$. Therefore, crystal B1 is identified as crystal orientation C with the unit cell's edge length a and b . As two crystals are investigated, one can also know beforehand which crystal plane is orientation B with unit cell's edge length a and c .

In short, the sample preparation method was successful for both absorption spectroscopy and electron diffraction; crystallised rubrene shows $\Delta\lambda_r = 5$ nm redshifted equidistant absorption peaks of $\Delta k = 1350 \text{ cm}^{-1}$ from which $\lambda = 536$ nm is the most effective wavelength to excite the rubrene crystal; and crystal A3 is identified as crystal orientation A, Fig. 2.7a, crystal B1 is identified as crystal orientation C, Fig. 2.7c.

7 Outlook

This research has been successful to map the absorption spectra of both dissolved and crystallised rubrene. From these absorption spectra vital information has been extracted of the efficient excitation wavelengths of the molecular crystal. This information has been used in another part of the research where a femtosecond laser pulse beam is moderated in such a way that the input wavelength $\lambda = 800$ nm can be changed to (approximately) the most efficient excitation wavelength of rubrene in order to excite the crystal. The output wavelength of the laser was eventually altered to $\lambda = 529$ nm [22]. A peak wavelength that approximates the lowest energetic absorption band of rubrene rather well.

Furthermore, this research has observed two out of three crystal orientation for an orthorhombic side-centred rubrene crystal. Meaning, that all orientation of the rubrene crystal are now known. Eventually, when taking electron diffraction images at higher energies, the orientation of the examined crystal sample will be well known.

The ground state of rubrene is characterised on its absorption spectrum and electron diffraction patterns. In addition, the laser set-up for the excitation laser pulse had been properly aligned and characterised. Building on this work and [22], the overall research can start conducting time-resolved TAS and UED experiments to study the behaviour of organic rubrene crystals from 10 K up to room temperature. This is, however, just the beginning of the research. Even more fascinating molecular crystals can be investigated in the home-built diffractometer once their ground state is well known.

When exciting the rubrene crystal, one must always keep in mind that it is an anisotropic crystal. Meaning, its absorption is polarisation dependent. In addition, the crystal slices are applied on the TEM meshes with unknown rotation. If the absorption direction of the examined crystal is not known, the crystal can remain unexcited during the experiments. A possibility to solve this particular problem is to depolarise the laser pulse with a diffuser for example. This, however, also introduces dispersion and loss of light intensity. Another option is to apply an aperture on every sample slice and determine the most efficient polarisation direction for light absorption per sample. When it is known, one can alter the polarisation of the excitation laser pulse with a waveplate.

8 Bibliography

- [1] Kenneth S. Krane, *Modern Physics*, English, Third edition. John Wiley & Sons, inc, 2012, ISBN: 978-1-118-06114-5.
- [2] Peter Atkins, Julio de Paula, James Keeler, “Physical Chemistry,” English, in 11th Edition. Oxford, 2018, ch. 9 Molecular Structure, ISBN: 978-0-19-876986-6.
- [3] Lecture notes of ‘Applied Science Chemie’. “Elektronendelocalisatie en -resonantie.” Dutch. Unpublished. (2021).
- [4] Peter Atkins, Julio de Paula, James Keeler, “Physical Chemistry,” English, in 11th Edition. Oxford, 2018, ch. 15A Solids, Crystal Structure, ISBN: 978-0-19-876986-6.
- [5] Technische Universität Braunschweig. “Electronic Transitions.” English. (2022), [Online]. Available: http://www.ptb.de/aggericke/PC4e/Kap_III/Elektronischer_Uebergang.htm (visited on 04/13/2022).
- [6] Peter Atkins, Julio de Paula, James Keeler, “Physical Chemistry,” English, in 11th Edition. Oxford, 2018, ch. 11 Molecular Spectroscopy, ISBN: 978-0-19-876986-6.
- [7] Dr. Bart Smit, *Lecture notes of ‘Moleculufysica’*, Dutch, Unpublished, Eindhoven, 2021.
- [8] Dr. Heinrich Schwoerer, “Basics of Diffraction,” English, March 2013, Unpublished.
- [9] Matthew Schwartz, “Diffraction and resolution,” English, [Online]. Available: <https://scholar.harvard.edu/files/schwartz/files/lecture19-diffraction.pdf>.
- [10] Leica Microsystems, The new Ultramicrotome for Room Temperature and Cryosectioning. English. (2016), [Online]. Available: https://downloads.leica-microsystems.com/Leica%20EM%20UC7/Brochures/Leica%20EM%20UC7_FC7%20Brochure%20V2016-02%20Screen_EN.pdf (visited on 04/13/2022).
- [11] DiAtome, diamond knives. English. (2021), [Online]. Available: https://www.diatomeknives.com/knives/pdf/DiATOME_EMS_2019.pdf (visited on 04/13/2022).
- [12] Rowaco, Perfect loop. English. (2020), [Online]. Available: <https://rowaco.se/en/item/ptxl-powertome-ultramicrotome/> (visited on 04/29/2022).
- [13] Avantes, AvaSpec-ULC2048CL-EVO. English. (2020), [Online]. Available: https://avantes.b-cdn.net/content/uploads/2020/08/DS-Spec-AvaSpec-ULS2048CL-EVO-21072.pdf6_.pdf (visited on 05/24/2022).
- [14] Ocean Insight, DH-2000-BAL Light Source. English. (2017), [Online]. Available: <https://www.oceaninsight.com/products/light-sources/uv-vis-nir-light-sources/dh-2000-bal/?qty=1> (visited on 05/24/2022).
- [15] National Center for Biotechnology Information (2022). “Compound Summary for CID 6212, Chloroform.” English. (April 2022), [Online]. Available: <https://pubchem.ncbi.nlm.nih.gov/compound/Chloroform> (visited on 04/27/2022).
- [16] —, “PubChem Compound Summary for CID 68203, Rubrene.” English. (April 2022), [Online]. Available: <https://pubchem.ncbi.nlm.nih.gov/compound/Rubrene>. (visited on 04/27/2022).
- [17] Huang, Liwei and Liao, Qing and Shi, Qiang and Fu, Hongbing and Ma, Jinshi and Yao, Jiannian, “Rubrene micro-crystals from solution routes: Their crystallography, morphology and optical properties,” English, *J. Mater. Chem.*, vol. 20, pp. 159–166, 1 2010. DOI: 10.1039/B914334C. [Online]. Available: <http://dx.doi.org/10.1039/B914334C>.
- [18] Thermo Scientific, NanoDrop 2000c. English. (2009), [Online]. Available: <https://assets.fishersci.com/TFS-Assets/CAD/Specification-Sheets/D17050~.pdf> (visited on 05/24/2022).
- [19] Ma, Lin and Zhang, Keke and Kloc, Christian and Sun, Handong and Michel-Beyerle, Maria E. and Gurzadyan, Gagik G., “Singlet fission in rubrene single crystal: Direct observation by femtosecond pump–probe spectroscopy,” English, *Phys. Chem. Chem. Phys.*, vol. 14, pp. 8307–8312, 23 2012. DOI: 10.1039/C2CP40449D. [Online]. Available: <http://dx.doi.org/10.1039/C2CP40449D>.

- [20] T. Petrenko, O. Krylova, F. Neese, and M. Sokolowski, “Optical absorption and emission properties of rubrene: Insight from a combined experimental and theoretical study,” English, *New Journal of Physics*, vol. 11, no. 1, p. 015 001, January 2009. DOI: 10.1088/1367-2630/11/1/015001.
- [21] Thorlabs, Polarisation Filter LPVISE100-A. English. (Jul. 2010), [Online]. Available: <https://www.thorlabs.com/thorproduct.cfm?partnumber=LPVISE100-A> (visited on 05/05/2022).
- [22] Aeden Nikei Lindelauf, “Characterisation and Propagation of a Femtosecond Laser Pulses,” English, Max Planck Institute for the Structure and Dynamics of Matter & Fontys University of Applied Sciences, Jun. 2022.
- [23] Douglas C. Giancoli, *Physics for Scientists & Engineers with Modern Physics*, English, 4th Edition. Pearson, 2009, ISBN: 978-0-13-149508-1.
- [24] Matthew Schwartz, “Antennas and interference,” English, [Online]. Available: <https://scholar.harvard.edu/files/schwartz/files/lecture18-antennas.pdf>.

Epilogue

It was a genuine honour to have been given the chance to intern at the Max Planck Institute for the Structure and Dynamics of Matter. I made optimally use of the experience and have learned many valuable things about academia and myself.

I am inclined to thank everyone again who has helped and guided me during this time abroad. And of course, the everlasting support from friends and family must not go unnamed.

With this said, I want to conclude my thesis.

Appendix A: Hybridisation of Carbon Atoms

As mentioned in Ch. 2, carbon has the following electron configuration: $[\text{He}]2s^22p^2$. In Fig. A.1 a schematic image of this electron configuration is shown.

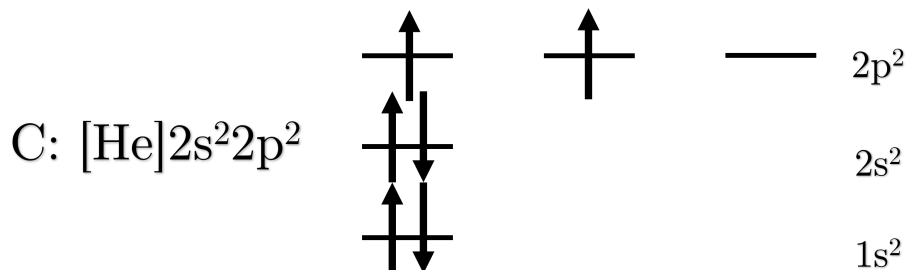


Figure A.1: A schematic representation of the electron configuration according to valence bond theory.

The arrows represent the electrons on certain energy levels and states. An arrow up means that the electron has a magnetic spin quantum number of $+\frac{1}{2}$, an arrow down the opposite, $-\frac{1}{2}$. The electrons in this configuration still follow the Pauli exclusion principle and Hund's maximum multiplicity rule.

According to the valence bond theory, carbon would be able to bind merely two times. This is however one of the many shortcomings of the valence bond theory. Molecular orbital theory considers more variables which makes hybridisation possible. In this appendix, the hybridisation of the carbon atom will be discussed and will give an explanation for the common tetravalence of carbon. First of all, carbon can hybridise in three ways for organic compounds, all of which will be discussed in this appendix for completeness. Yet carbon only contains the sp^2 -hybridisation in benzene rings and thus in rubrene too. So the reader could skip the sp - and sp^3 -hybridisation and read the necessary information of sp^2 -hybridisation.

sp^3 -Hybridisation

sp^3 -hybridisation will be discussed first as it is the carbon hybridisation which is found in alkanes, the simplest organic compounds. Take methane, CH_4 for example, it has a carbon atom and four hydrogen atoms. Four hydrogen atoms indicate that all orbitals must be bound linearly with a σ -bond. Intuitively, one can imagine that p-orbitals would energetically be unfavourable relatively to sp-orbitals. The s-electrons are promoted while the p-electrons are slightly degraded, all forming sp-orbitals. The electron configuration of sp^3 -hybridised carbon atoms is depicted in Fig. A.2.

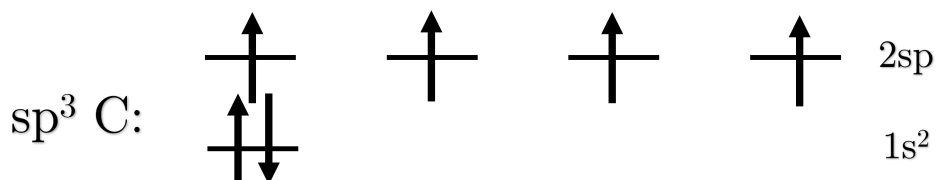


Figure A.2: The electron configuration of a sp^3 -hybridised carbon atom. Here can be seen that two s-electrons have been promoted to sp-electrons and that two p-electrons have been demoted to sp-electrons.

The hybridisation of an s- and a p-electron creates a sort of balloon-like shape which is a combination of a s-orbital and p-orbital. As discussed, this means for sp^3 -hybridisation that carbon will obtain four sp-orbitals. In Fig. A.3 an image is displayed of the sp^3 -hybridisation of carbon.

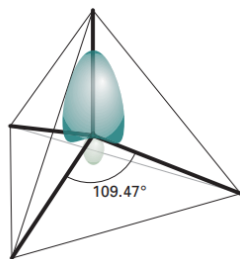


Figure A.3: This figure depicts a sp^3 -hybridised carbon atom. The black lines represent the sp -orbital which is illustrated for the vertical orbital. [2]

As can be seen in the illustration, the sp -orbitals are tilted 109.5° relatively to each other. This is the energetically most favourable orientation where the Coulomb interactions are minimal.

sp^2 -Hybridisation

The carbon atoms in benzene rings are sp^2 -hybridised. It is also the hybridisation found in alkene molecules such as ethylene, C_2H_4 . A characteristic of Alkene compounds is the double covalent bond between two carbon atoms instead of one. This type of binding would not be possible with sp^3 -hybridisation as that would require two σ -bonds, linear bonds, on the same location. Instead, three electrons bind linearly and one non-linearly. That would mean the carbon atoms in ethylene each have three σ -bonds and a single π -bond. This new electron configuration is schematically depicted in Fig. A.4.

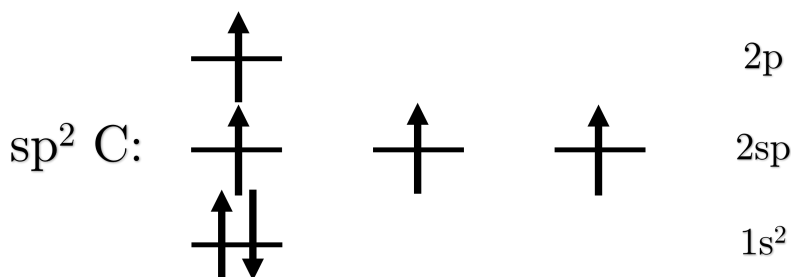


Figure A.4: The electron configuration of a sp^2 -hybridised carbon atom. Here can be seen that two s -electrons have been promoted to sp -electrons and that only one p -electrons has been demoted to sp -electrons. The last p -electron remains in its original state.

The p -orbital will be considered vertically, the three remaining sp -orbitals will be orientated such that the Coulomb interaction is minimal. This is on the horizontal plane from the nucleus at an angle of 120° from each other. In Fig. A.5 an illustration of sp^2 -hybridisation of carbon is depicted.

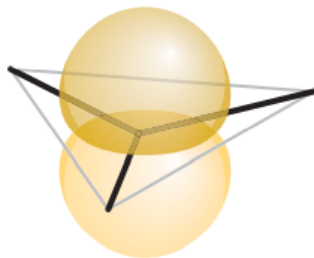


Figure A.5: This figure depicts a sp^2 -hybridised carbon atom. The black lines represent the sp -orbital, whereas the yellow shapes represents the p -orbital. [2]

sp-Hybridisation

Alkane and alkene compounds are discussed, but there is one more organic compound, one that uses sp-hybridisation: alkynes. Lets take ethyne, C_2H_2 for example. This molecule is similar to ethylene. The carbon atoms of Ethylene were double bonded, in ethyne the carbon are triple bonded. Again, multiple linear σ -bonds is impossible. To resolve this, the carbon atoms must share two π -bonds and a single σ -bond. In Fig. A.6 a schematic image of the sp-hybridised carbon atom is displayed.

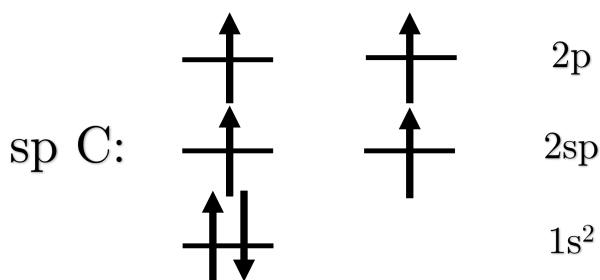


Figure A.6: The electron configuration of a sp-hybridised carbon atom. Here can be seen that two s-electrons have been promoted to sp-electrons and that no p-electrons have been demoted to sp-electrons. The p-electrons remain in their original state.

When one p-orbitals is considered vertically, then the other will automatically be located horizontally. The sp-orbitals will naturally be perpendicular on both and opposite or 180° to each other. A schematic image of the structure of a triple bond in ethyne is depicted in Fig. A.7.

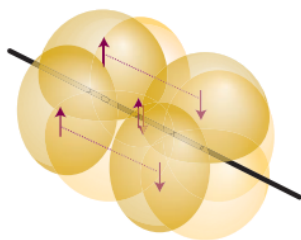


Figure A.7: This figure depicts the bonds of an ethyne molecule where the carbon atoms are sp-hybridised. The black lines still represent the sp-orbital that don't bind to the carbon, whereas the yellow shapes represents the π -bonds and σ -bond of the carbon atoms. [2]

Appendix B: Crystal Unit Cells

In Ch. 2, the unit cell is mentioned. However, Par. 2.1 only discussed the Rubrene unit cell, orthorhombic side-centred. The unit cell is a useful way to model crystals as they are the fundamental ‘building block’ of crystallised matter.

This appendix will further discuss the unit cells. For this, the same table is presented here as in Par. 2.1.

Table B.1: An overview of the possible unit cells in a crystal with the corresponding edge lengths and internal angles.

Unit cells	Edge lengths	Internal angles
Cubic	$a = b = c$	$\alpha = \beta = \gamma = 90^\circ$
Tetragonal	$a = b \neq c$	$\alpha = \beta = \gamma = 90^\circ$
Orthorhombic	$a \neq b \neq c$	$\alpha = \beta = \gamma = 90^\circ$
Monoclinic	$a \neq b \neq c$	$\alpha = \beta = 90^\circ \neq \gamma$
Trigonal	$a \neq b \neq c$	$\alpha \neq \beta \neq \gamma \neq 90^\circ$
Triclinic	$a \neq b \neq c$	$\alpha \neq \beta \neq \gamma \neq 90^\circ$
Hexagonal	$a = b \neq c$	$\alpha = \beta = 90^\circ \neq \gamma = 120^\circ$

First, the cubic unit cell is discussed. The cubic unit cell is the easiest cell possible. The bond lengths of the lattices are in every direction equal, idem dito for the internal angles which are all 90° . These mathematical properties makes this unit cell a cube. Although, more variants of the cubic unit cell are possible: body-centred and face-centred. All cubic unit cells are illustrated in Fig. B.1.

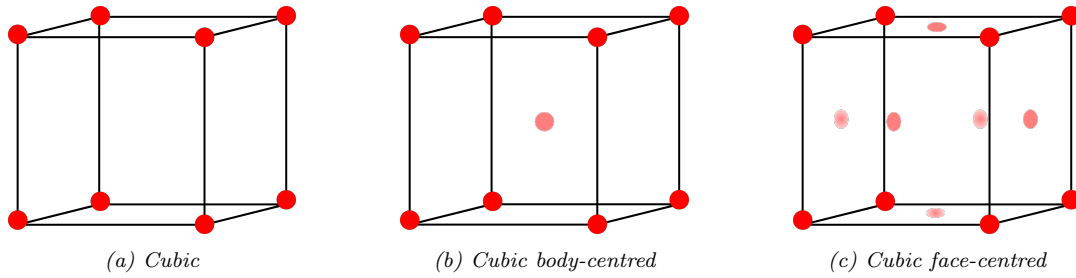


Figure B.1: Three possibilities of cubic latticed unit cells.

The red dots in the illustrations of Fig. B.1 represent the lattices of atoms or molecules. In Fig. B.1b an extra lattice is added in the centre of the cube, while in Fig. B.1c all planes have an extra lattice.

When a cube is stretched a more cuboid shape is created. This is the case with the tetragonal unit cell: one two edges are equal, but one is extended. The internal angles however all remain equal. There are two possible tetragonal unit cells: the simple tetragonal and body-centred. Fig. B.2 shows illustrations of these unit cells.



Figure B.2: Two possibilities of tetragonal latticed unit cells.

Fig. B.2a merely shows a stretched version of Fig. B.1a. The same is true for Fig. B.2b and Fig. B.1b. It is, however, not possible to create a face-centred tetragonal. A face-centred tetragonal unit cell would simply be able to be divided in another, smaller, unit cell.

When stretching the tetragonal unit cell in another dimension, the orthorhombic unit cells is obtained. This indicates that orthorhombic does not have any equal edges. Still, the internal angles are all equal 90° . Orthorhombic unit cells can be divided in four separate categories: simple orthorhombic, body-centred, face-centred, and side-centred. All are depicted in Fig. B.3.

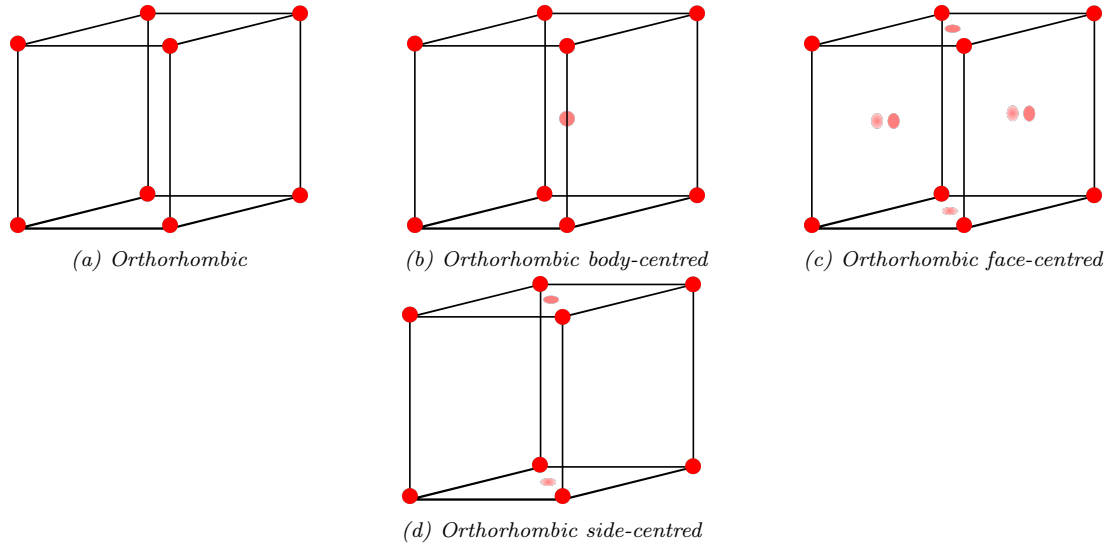


Figure B.3: Four possibilities of orthorhombic latticed unit cells.

Orthorhombic is just another cuboid shape. Fig. B.3b again shows a body-centred unit cell where an extra lattice is in the centre of the cuboid and Fig. B.3c shows a face-centred unit cell where lattices are added on every plane. However, there is a new type of cell, side-centred, Fig. B.3d. Extra lattices are added on the top and bottom plane. This is actually the unit cell with which rubrene is crystallised.

A cube or cuboid can not only be stretched, it can also be sheared creating a parallelepiped. A parallelepiped is a three dimensional parallelogram. In the parallelepiped unit cells no equal edges are allowed, that would make it possible to divide the unit cell in other smaller unit cells. But the internal angles are now adjusted. Monoclinic, for example, still has two internal angles which equal 90° , but also has one angle which does not equal 90° . Also, it is possible for the monoclinic unit cell to be side-centred. Schematic images of these unit cells are presented in Fig. B.4.

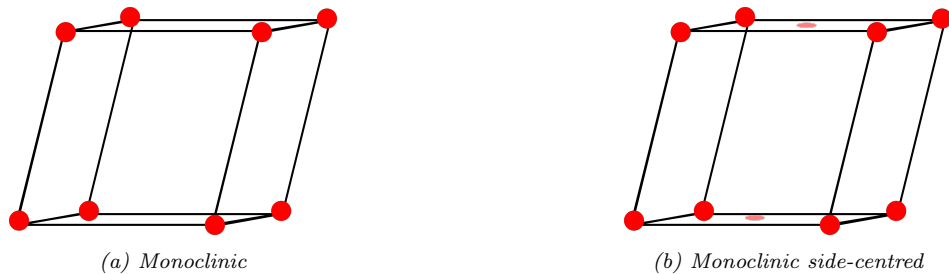


Figure B.4: Two possibilities of monoclinic latticed unit cells

Monoclinic unit cells can be regarded as sheared orthorhombic cells. Side-centred cell, Fig. B.4b, again, show an extra lattice at the top and bottom plane of the parallelepiped.

The internal angles do not necessary have to equal each other. In the case of no equal edges and no equal internal angles, a triclinic unit cell is obtained. Triclinic, however, does not have subcategory unit cells. An illustration of the triclinic unit cell is depicted in Fig. B.5

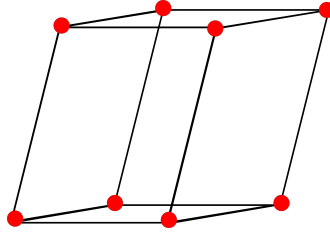


Figure B.5: The triclinic latticed unit cell.

This shape is merely an shear of the orthorhombic unit cell in two directions, or a shear of the monoclinic in one direction.

Lastly, a shape that is neither cuboid not parallelepiped: the hexagonal unit cell. The hexagonal unit cell must have two equal edges, two internal angles equalling 90° , and one internal angle equalling 120° . Also here, no subcategories are allowed. A schematic picture of this unit cell is shown in Fig. B.6.

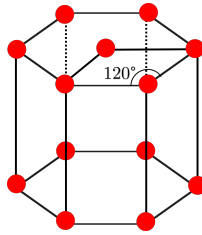


Figure B.6: The hexagonal latticed unit cell.

The unit cell is merely one piece of the hexagonal, which is shown in Fig. B.6. Combining three of these unit cells creates a hexagonal.

Appendix C: Derivation of Diffraction

In Par. 2.3 merely the outline of diffraction and the result of N-slit diffraction is discussed. However, it has much more physical and mathematical background. Also here, just Fraunhofer diffraction is considered. Single slit diffraction will be discussed first, then multi beam interference, and, lastly, the multi slit diffraction.

For electromagnetic waves, diffraction is caused by an obstacle such as an aperture or a slit where new Huygens waves will appear with incoming light. Instead of emitting a point like light source, the light waves will interfere, sometimes constructively, sometimes destructively. Which creates the characteristic maximum and minimum intensities on the focal plane. Fig. C.1 shows an illustration of diffraction from a single slit with an incident plane wave.

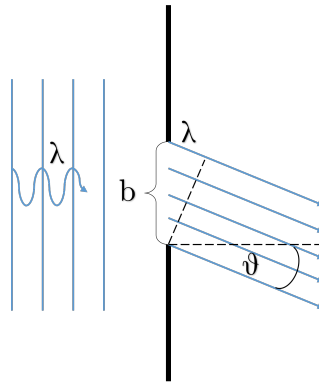


Figure C.1: An illustration of a single slit experiment with light.

The beam is scattered as half a sphere where the angle is given by θ , so that perpendicular to the slit entrance would be $\theta = 0^\circ$. As the optical path length of each wave that exits the slit on an angle is not equal to its neighbouring, there must be interference between the waves. The interference must also be destructive, minimal, when the distance d is half of the wavelength $d = \frac{\lambda}{2}$. Moreover, the interference must be constructive, when the distance d is a whole wavelength $d = \lambda$. The distance can also be given by simple trigonometry: $d = b \sin(\theta)$. This gives:

$$b \sin(\theta) = m\lambda, \quad m \in \mathbb{Z}, \quad m \neq 0, \quad (\text{C.1})$$

when interfering destructively at minima, and

$$b \sin(\theta) = \frac{m}{2}\lambda, \quad m \in \mathbb{Z}, \quad m \neq 1. \quad (\text{C.2})$$

These are some of the characteristics one can see on the focal plane. Eq. C.1 and Eq. C.2 only can have practical application such as measuring thicknesses. However, not only the maxima and minima are required, also the electric field and intensity of the light is desired.

Single Slit Diffraction

There are two possible ways to derive expressions for the electric field and intensity: mathematically and physically. From a physical point of view, diffraction is an interference of waves; from a mathematical view, diffraction is merely the Fourier transform of the slit.

Mathematical

For the mathematical derivation, the function that must be transformed first needs to be known, which is surprisingly simple. Remember the assumptions that are made in Par. 2.3: the incident beam is a plane wave. So, the function that must be transformed is actually a single block wave

with a certain width. To start, the definition of Fourier transform is given:

$$\mathfrak{F}\{f(x)\} = \int_{-\infty}^{\infty} f(x)e^{-ikx}dx. \quad (\text{C.3})$$

Lets assume the value of the block signal is just the amplitude of the electric field. The signal function will look like:

$$E(x) = \begin{cases} E_0 & -\frac{b}{2} \leq x \leq \frac{b}{2} \\ 0 & \text{otherwise} \end{cases} \quad (\text{C.4})$$

To calculate the Fourier transform of this signal the exponent $\exp(-ikx \sin(\theta))$ is used in the transform integral. The factor of $\sin(\theta)$ is added to account for all angles the beam is headed. This gives the following integral:

$$E(\theta) = \frac{1}{b} \int_{-\frac{b}{2}}^{\frac{b}{2}} E_0 e^{-ikx \sin(\theta)} dx. \quad (\text{C.5})$$

Solving this gives an expression for the electric field as a function of the angle:

$$E(\theta) = E_0 \frac{\sin\left(k\frac{b}{2} \sin(\theta)\right)}{k\frac{b}{2} \sin(\theta)}, \quad (\text{C.6})$$

or

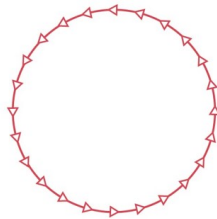
$$E(\theta) = E_0 \frac{\sin\left(\frac{\pi}{\lambda} b \sin(\theta)\right)}{\frac{\pi}{\lambda} b \sin(\theta)}. \quad (\text{C.7})$$

This delivers a sinc function. Yet electric field is not measured, the intensity is. So, the electric field must be squared.

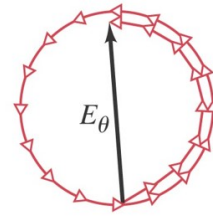
$$I(\theta) = I_0 \left(\frac{\sin\left(\frac{\pi}{\lambda} b \sin(\theta)\right)}{\frac{\pi}{\lambda} b \sin(\theta)} \right)^2. \quad (\text{C.8})$$

Physical

Another point of view is by regarding phasors of the Electric field. This is schematically represented by Fig. C.2.



(a) Phasors of destructive interference.



(b) Phasors of constructive interference.

Figure C.2: The electric field continuously shifts phase resulting in interference. Sometimes constructively, sometimes destructively. Fig. C.2a represents destructive interference as there is no electric field vector. Fig. C.2b represents constructive interference as the image shows the largest electric field possible. [23]

Fig. C.2a represents the situation of deconstructive interference and Fig. C.2b represents the situation of constructive interference, in this figure a vector is drawn which depicts the effective electric field E_θ . Every single Huygens wave that exits the slit adds to this phasor diagram. When assuming there is an infinite amount the phasor diagram will become continuous instead of discrete, this is shown in Fig. C.3.

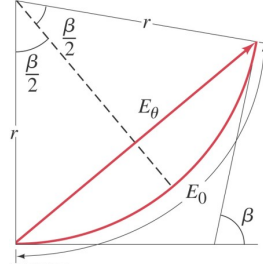


Figure C.3: A part of a phasor diagram where E_0 is the total continuous electric field. [23]

The angle the electric field has rotated is described by β . From anywhere in the circle a perpendicular line can be drawn from the centre to the vector. The angle between the base of the vector and the intercept is $\frac{\beta}{2}$. By applying simple trigonometry the following relation is found:

$$\frac{E_\theta}{2} = r \sin\left(\frac{\beta}{2}\right). \quad (\text{C.9})$$

It is known that the arc of a circle is given by the radius times the angle, this mathematical relation will be applied to find an expression for the radius r :

$$r = \frac{E_0}{\beta}. \quad (\text{C.10})$$

By combining Eq. C.9 with Eq. C.10 the following equation is obtained:

$$E(\theta) = E_0 \frac{\sin\left(\frac{\beta}{2}\right)}{\frac{\beta}{2}}. \quad (\text{C.11})$$

As it is the intensity that is measured not the electric field, Eq. C.11 must be squared.

$$I(\theta) = I_0 \left(\frac{\sin\left(\frac{\beta}{2}\right)}{\frac{\beta}{2}} \right)^2 \quad (\text{C.12})$$

There still is no expression for β . Beta is as the difference of the optical path length between two neighbouring Huygens waves multiplied by the wavenumber. As the difference is also equal to the length of the slit entrance multiplied by the sine of the angle, and the wave number is defined as $\frac{2\pi}{\lambda}$, an expression for β is obtained:

$$\beta = \frac{2\pi}{\lambda} b \sin(\theta). \quad (\text{C.13})$$

Substituting Eq. C.13 into Eq. C.12 gives:

$$I(\theta) = I_0 \left(\frac{\sin\left(\frac{\pi b \sin(\theta)}{\lambda}\right)}{\frac{\pi b \sin(\theta)}{\lambda}} \right)^2, \quad (\text{C.14})$$

or the sinc function squared. The calculated electric field and the intensity is plotted and shown in Fig. C.4.

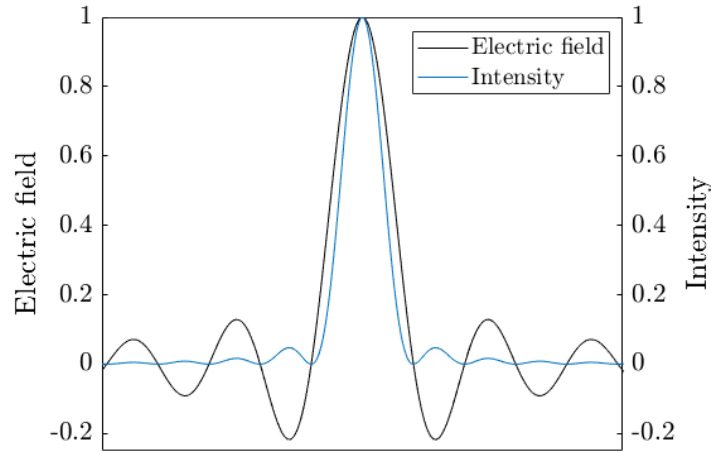


Figure C.4: A normalised example of the sinc function for the electric field (the blue graph) and the sinc function squared for the intensity (the orange graph). Note that the electric field can reach below zero which would never be possible for the intensity as intensity must be greater than zero. The intensity only shows positive maxima and minima which equal zero.

The intensity graph is the better representation what one would see on a screen. The graph clearly shows periodical maxima and minima.

Multi Beam Interference

The previous paragraph regarded adjacent Huygens waves which created the single slit. Now, those holes are not connected, but separated with a distance s . Because the holes are assumed to be infinitesimal, one can write the outgoing electric field as a summation of all Huygens waves with an additional phase shift (under the assumption that the amplitude of the electric field is equal for every Huygens wave). This results in the next relation [8, 9, 24]:

$$\begin{aligned} E &= E_0 e^{-i\omega t + ikx} \left[1 + e^{-i\Delta} + e^{-i2\Delta} + e^{-i3\Delta} + \dots + e^{-i(N-1)\Delta} \right], N \in \mathbb{N} \\ &= E_0 e^{-i\omega t + ikx} \sum_{n=0}^{N-1} e^{-in\Delta}. \end{aligned} \quad (\text{C.15})$$

Here, a complex wave function (in space and time) is used to describe the electric field. The summation of the individual Huygens waves at the total amount of N which must be a positive integer. The phase shift is represented by Δ and is equal to $\Delta = \frac{2\pi}{\lambda} s \sin(\theta)$, where s is the distance between slits. Using the geometrical series [9, 24]

$$\sum_{n=0}^{N-1} a^n = \frac{1 - a^N}{1 - a}, \quad (\text{C.16})$$

so that

$$E = E_0 e^{-i\omega t + ikx} \frac{1 - e^{-iN\Delta}}{1 - e^{-i\Delta}}. \quad (\text{C.17})$$

By multiplying the fraction with two others, the expression can be simplified to a fraction of sines by using its complex definition [8, 24].

$$\begin{aligned}
 E &= E_0 e^{-i\omega t + ikx} \frac{1 - e^{-iN\Delta}}{1 - e^{-i\Delta}} \cdot \frac{e^{i\frac{N}{2}\Delta}}{e^{i\frac{N}{2}\Delta}} \cdot \frac{e^{i\frac{\Delta}{2}}}{e^{i\frac{\Delta}{2}}} \\
 &= E_0 e^{-i\omega t + ikx} \frac{e^{i\frac{N}{2}\Delta} - e^{-i\frac{N}{2}\Delta}}{e^{i\frac{\Delta}{2}} - e^{-i\frac{\Delta}{2}}} \frac{e^{i\frac{N}{2}\Delta}}{e^{i\frac{\Delta}{2}}} \\
 &= E_0 e^{-i\omega t + ikx} \frac{\sin(\frac{N}{2}\Delta)}{\sin(\frac{\Delta}{2})} \frac{e^{i\frac{N}{2}\Delta}}{e^{i\frac{\Delta}{2}}}.
 \end{aligned} \tag{C.18}$$

As the physical electric field only exists in the real domain, the real part of the expression is taken. The remaining exponents will become a combined cosine. Which, after averaging, becomes vanishes from the expression, leaving the sine fraction and the amplitude of the electric field. [8, 9, 24]

$$E(\theta) = E_0 \frac{\sin(\frac{N}{2}\Delta)}{\sin(\frac{\Delta}{2})} = E_0 \frac{\sin(\frac{N\pi}{\lambda} s \sin(\theta))}{\sin(\frac{\pi}{\lambda} s \sin(\theta))} \tag{C.19}$$

The electric field squared gives an expression for the intensity:

$$I(\theta) = I_0 \left(\frac{\sin(\frac{N\pi}{\lambda} s \sin(\theta))}{\sin(\frac{\pi}{\lambda} s \sin(\theta))} \right)^2 \tag{C.20}$$

In the Fig. C.4, the electric field and intensity of multi beam interference is plotted for multiple values of N .

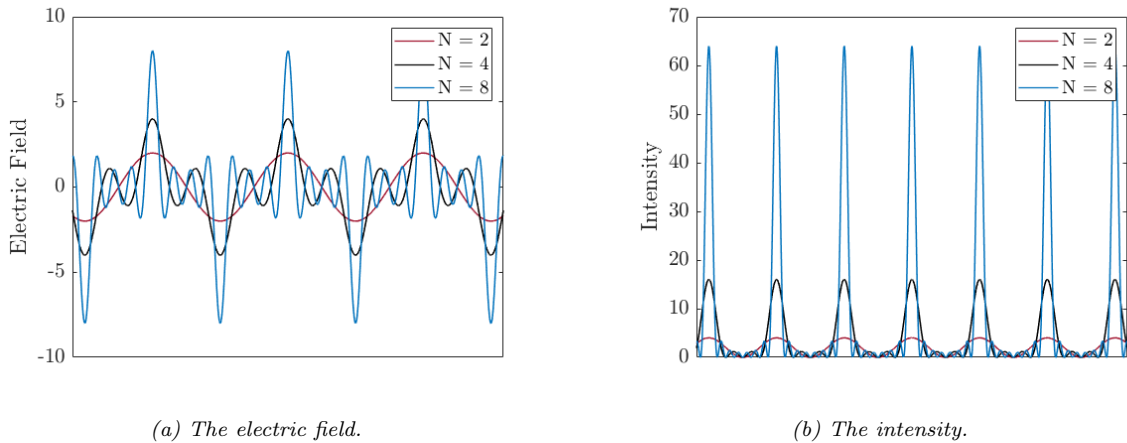


Figure C.5: The resulting electric field (Fig. C.5a) and intensity (Fig. C.5b) of multi beam interference for $N = 2, 4, 8$ Huygens waves.

As one can see in the when $N = 1$ the electric field is merely equal to its amplitude. Only with $N > 1$ can interference occur. The same is true for the intensity. Also noticeable, is that every maxima seems to be on the same height, regardless of the total amount of Huygens waves. This is due to the fact that the denominator is also a sine function. Earlier with the sinc function, the denominator was the same variable as in the sine function. The maxima, however, do not seem to shift with the total amount of Huygens waves.

Multi Slit Diffraction

To extend the model of multi beam interference to multi slit diffraction, it has to be combined with single slit diffraction. This is surprisingly simple, as the two model must merely be multiplied with each other [8]. The resulting electric field and intensity are given by:

$$E(\theta) = E_0 \frac{\sin(\frac{\pi}{\lambda} b \sin(\theta))}{\sin(\frac{\pi}{\lambda} s \sin(\theta))} \frac{\sin(\frac{N\pi}{\lambda} s \sin(\theta))}{\sin(\frac{\pi}{\lambda} s \sin(\theta))} \tag{C.21}$$

$$I(\theta) = I_0 \left(\frac{\sin\left(\frac{\pi}{\lambda} b \sin(\theta)\right)}{\frac{\pi}{\lambda} b \sin(\theta)} \right)^2 \left(\frac{\sin\left(\frac{N\pi}{\lambda} s \sin(\theta)\right)}{\sin\left(\frac{\pi}{\lambda} s \sin(\theta)\right)} \right)^2 \quad (\text{C.22})$$

Plotting these function gives the result shown in Fig. C.6. The electric field and intensity are calculated and plotted for $N = 8$ slits. The sinc function (squared) is the envelope of the calculated function, which is represented by the dashed line. Also, when $N = 1$, one can notice that the right term will be equal to 1, leaving the sinc function squared for the intensity, or single slit diffraction.

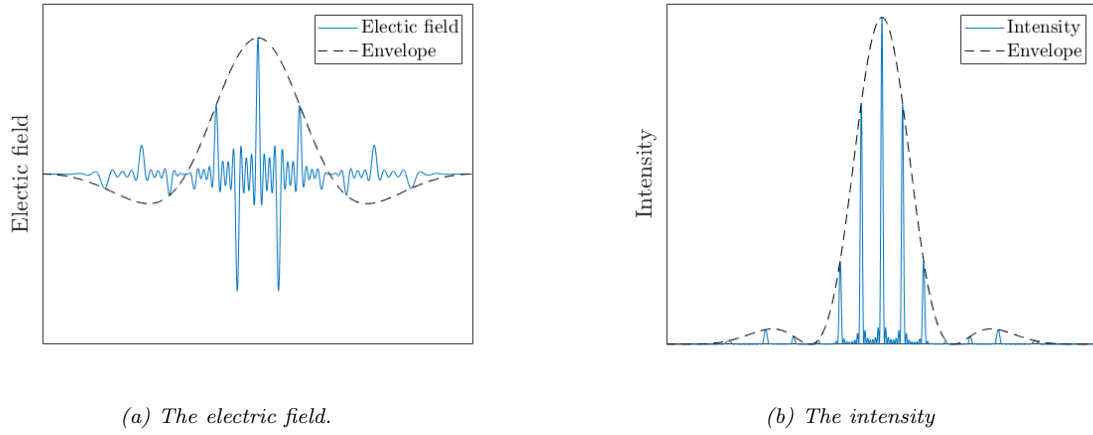


Figure C.6: The resulting electric field (Fig. C.6a) and intensity (Fig. C.6b) of multi slit diffraction for $N = 8$ slits. The values are not drawn as they differ in each situation.